batteries

MDPI

Review

Metaheuristic Optimization and Artificial Intelligence for Lithium-Ion Battery Modelling, Parameter Identification, and State Estimation: A Critical Review

Ahmed M. Nassef [1,*], Hossam Magdy Balaha [2] and Mostafa A. Elhosseini [3]

[1] Department of Electrical Engineering, College of Engineering in Wadi Alddawasir, Prince Sattam Bin Abdulaziz University, Wadi Alddawasir 11991, Saudi Arabia
[2] Bioengineering Department, J.B. Speed School of Engineering, University of Louisville, Louisville, KY 40292, USA; hmbala01@louisville.edu
[3] Computers and Control Systems Engineering Department, Faculty of Engineering, Mansoura University, Mansoura 35516, Egypt; melhosseini@mans.edu.eg
* Correspondence: a.nasef@psau.edu.sa

Abstract

The validity of the models incorporated into battery management systems (BMSs) is crucial to the safe and effective use of lithium-ion batteries (LIBs), the predominant electrochemical energy storage technology for electric vehicles (EVs) and stationary storage. Over the past ten years, two methodological families have transformed battery modeling and diagnostics: artificial intelligence (AI) models that learn state estimators directly from data and metaheuristic optimization algorithms that recast parameter identification as a black box optimization problem. This paper critically and comprehensively analyzes both families. This paper first examines the primary battery model classes, integer-order and fractional-order equivalent circuit models (ECM/FO-ECMs) and electrochemical models, and the identifiability problems that underpin any identification process. Second, the paper presents a critical synthesis of reported accuracy trends across standard datasets and driving profiles, along with a taxonomy of metaheuristic algorithms for battery parameter identification, including evolutionary, swarm-based, physics-based, and bio-inspired approaches. Third, AI-based methods for estimating state-of-charge (SOC) and state-of-health (SOH) are analyzed. These methods range from simple machine learning to deep recurrent and attention-based architectures, with a focus on the new class of hybrid physics-informed methods (physics-informed neural networks and neural ordinary differential equations coupled with ECMs). Fourth, the synergy between the two approaches (AI-assisted optimization and metaheuristic tuning of AI estimators) is examined. In addition, this review addresses the "novel algorithm inflation" impacting the metaheuristic literature, the implications of the no-free-lunch theorem, the frequent lack of statistical validation and fair benchmarking, and the discrepancy between reported laboratory accuracy and real-time feasibility in embedded systems. Lastly, research perspectives are suggested, such as hardware-aware hybrid estimators, standardized open benchmarks, and chemistry-transferable identification (LFP, NMC, sodium-ion). The most practical route to scalable, field-ready battery management systems is to incorporate physical structures into artificial neural network designs, moving from strictly data-driven models to physics-informed hybrid frameworks.

Keywords: lithium-ion battery; battery modeling; metaheuristic optimization; parameter identification; deep learning; physics-informed machine learning; battery management system

Check for updates

Received: 11 September 2026
Revised: 20 October 2026
Accepted: 23 October 2026
Published: 2 November 2026

Copyright: © 2026 by the authors. Licensee MDPI, Basel, Switzerland. This article is an open access article distributed under the terms and conditions of the Creative Commons Attribution (CC BY) license.

1. Introduction

1.1. Motivation and Scope

Lithium-ion batteries (LIBs) are a key component of the global energy transition, driven by the electrification of road transportation and the widespread use of renewable energy sources. The battery management system (BMS), whose primary functions are state-of-charge (SOC) estimation, state-of-health (SOH) tracking, power capability prediction, thermal management, and fault detection, all of which rely on a mathematical model of the cell, controls the battery's longevity, performance, and safety [1,2]. The safety margin, usable energy, and battery system lifetime are thus directly influenced by the accuracy of this model and the factors that feed into it.

The fidelity and complexity of battery models vary widely. Internal transport and kinetic phenomena are physically rigorously described by electrochemical models, such as the Doyle–Fuller–Newman (DFN) pseudo-two-dimensional model and its single-particle simplifications, at the expense of dozens of parameters that are challenging to determine from full-cell data [3,4]. On the other hand, equivalent circuit models (ECMs), which represent the cell using a small number of lumped electrical elements, strike an attractive balance between accuracy and computational cost, making them the standard models in embedded BMSs [5,6]. By replacing ideal capacitors with constant-phase elements, fractional-order ECMs (FO-ECMs) reproduce the anomalous diffusion dynamics observed in electrochemical impedance spectra with fewer parameters than high-order integer models [7,8].

In parallel, advances in deep learning and the availability of large-scale datasets have driven a second methodological wave: AI models that directly forecast SOC, SOH, and remaining useful life (RUL) from observable signals [9]. Recurrent architectures (LSTM) [10,11], convolutional networks [12], attention-based networks [13], Gaussian process regression [14], and, more recently, hybrid physics-informed approaches such as physics-informed neural networks (PINNs) [15], coupled with circuit or electrochemical backbones [16,17], all promise estimators that generalize beyond the training distribution while retaining physical interpretability.

Regardless of the specific model, parameter identification must be performed using empirical data. Due to the nonlinear, frequently non-convex, and occasionally ill-conditioned nature of the resulting optimization problems, gradient-free metaheuristic algorithms have gained popularity as identification tools. During the same period, there has been a rapid increase in the development of new metaphor-based algorithms, a trend that has attracted criticism within the optimization community [18,19]. Consequently, battery parameter identification lies at the intersection of two rapidly evolving research areas and often lacks a unified methodological standard.

1.2. Related Reviews, Research Gaps and Objectives

Several reviews have addressed various aspects of this landscape, including ECM parameter estimation strategies [20,21], machine learning for SOC estimation [22,23], deep learning for SOH [24,25], and AI approaches to health diagnostics [26], data-driven SOH estimation on real-world data [27] and modeling and state estimation of sodium-ion batteries [28]. Most surveys look at metaheuristic and AI research separately. They often do not assess how reproducible or well benchmarked the main studies are, and they rarely offer practical advice on choosing methods for specific BMS tasks. This review sets out to address these gaps with three main goals:

- Review of the AI-based estimation and metaheuristic identification approaches, including their combinations (surrogate models and hyperparameter optimization).
- A critical evaluation of the common weaknesses of these approaches, such as novel algorithms inflation, lack of data and statistical analysis, inconsistent measurements and metrics, and embedded implementation constraints.
- Propose a research agenda focused on transferring these approaches to emerging chemistries, such as sodium-ion.

1.3. Review Methodology and Paper Organization

This article presents a critical narrative review rather than a formal systematic review or meta-analysis. To promote transparency and reproducibility in literature coverage, we followed and reported a documented search and selection protocol wd using relevant elements of the PRISMA 2020 statement [29]. Table A1 summarizes the protocol. Because the primary studies differ a lot in chemistry, temperature, excitation profile, sampling rate, model order, parameter constraints, and validation protocol, we did not combine their numerical results. Instead, we organize the statements in this paper as follows:

1. We report single-study results, along with details on the chemistry, dataset, operating conditions, and metrics used in each source.
2. We identify multi-study trends only when at least three studies using similar model types and validation methods show a consistent pattern.

Tables in Section 4 include an evidence-type column that reflects this classification.

The rest of the paper is illustrated in Figure 1, which presents the section and subsection titles. Section 2 reviews battery model classes and identifiability. Section 3 examines metaheuristic parameter identification and concludes with a critical discussion of its open challenges. Section 4 reviews artificial intelligence approaches to SOC and SOH estimation, including hybrid physics-informed architectures, and concludes with a discussion of their open challenges. Section 5 analyzes the synergies between these two families and proposes a decision framework. Section 6 addresses cross-cutting methodological issues, Section 7 outlines future research directions, and Section 8 is a conclusion.

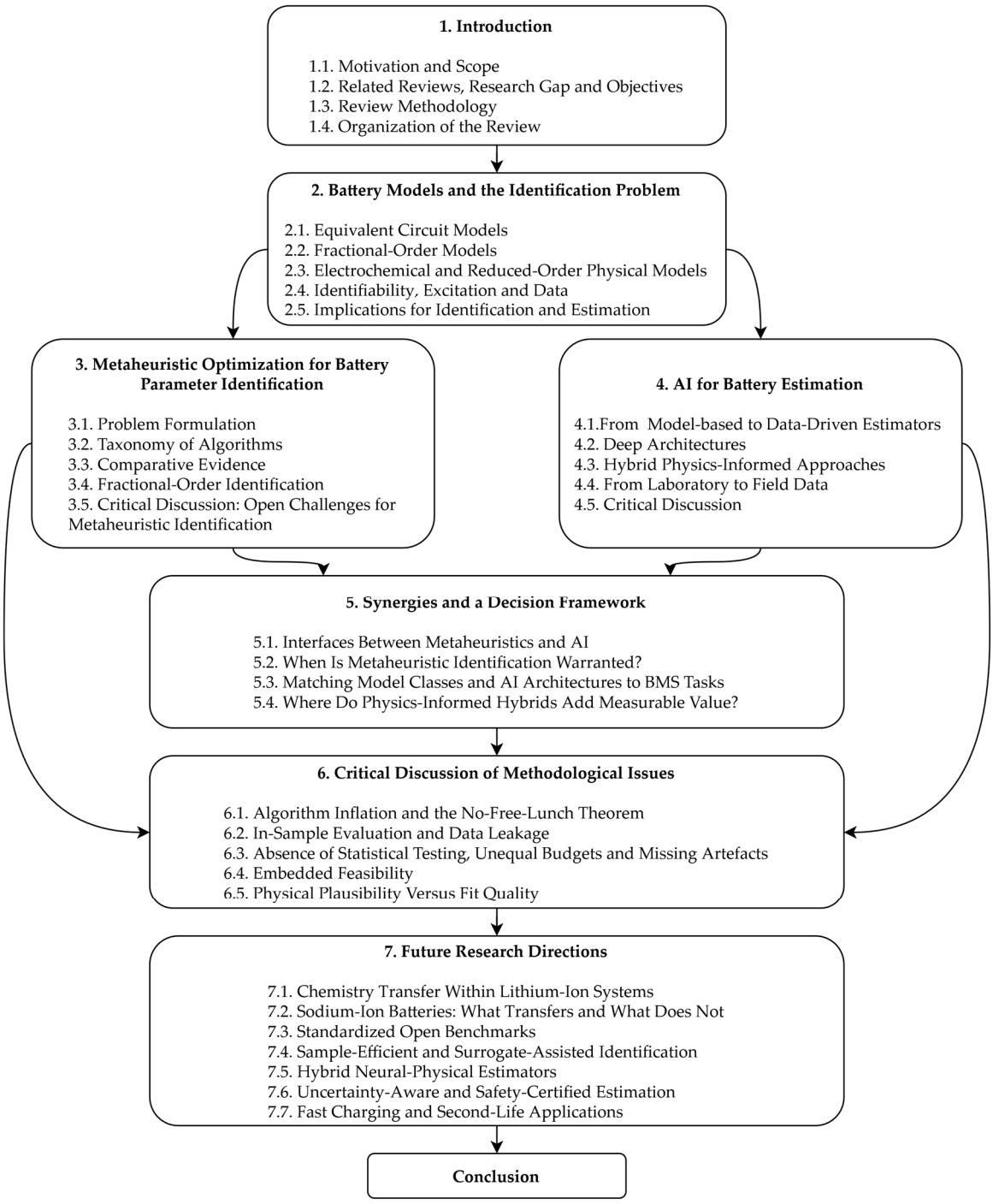


Figure 1. Overview schematic of the review scope.

2. Battery Models and the Identification Problem

2.1. Equivalent Circuit Models

An equivalent circuit model (ECM) represents the cell as an open-circuit voltage (OCV) source in series with an ohmic resistance (R_0) and n resistor–capacitor (RC) branches, which simulate charge-transfer and diffusion dynamics [5]. In discrete time, with a sampling period Δt, the terminal voltage of an nRC model is as follows:

$$v_t(k) = OCV(SOC(k), T) - R_0 i(k) - \sum_0^{j=n} v_{RC,j} \quad (1)$$

$$v_{RC,j}(k) = \exp\left(-\Delta t/\tau_{RC,j}\right) v_{RC}(k-1) + R_j\left[1 - \exp\left(-\Delta t/\tau_{RC,j}\right)\right];\ \tau_{RC,j} = R_j C_j \quad (2)$$

$$SOC(k) = SOC(k-1) + \eta \frac{i(k)\Delta t}{3600 Q_n} \tag{3}$$

where v_t denotes the terminal voltage (V), while $OCV(SOC(k), T)$ represents the open-circuit voltage as a function of SOC $\in [0, 1]$ and temperature T. R_0 refers to the ohmic resistance (Ω), and i indicates the cell current (A), which is positive during discharge. The variables v_j, R_j, C_j, and τ_j correspond to the polarization voltage, resistance, capacitance, and time constant of the jth RC branch, η denotes the Coulombic efficiency, and Q_n is the nominal capacity (Ah).

The model order is selected based on both cell chemistry and the intended application. He et al. [5] evaluated five ECMs and found that the dual-polarization model exhibited the best dynamic performance for the tested cells. Hu et al. [6], compared twelve ECMs on LiNMC and $LiFePO_4$ (LFP) cells and concluded that a first-order RC model was optimal for NMC cells, while adding a one-state hysteresis term improved performance for LFP cells. Nejad et al. [30] reported comparable results for both LFP and NMC chemistries. Tran et al. [31] assessed 1RC, 2RC, and 1RC-with-hysteresis models on LFP, NMC, LMO, and NCA cells and found that the optimal model structure depended on cell chemistry. Collectively, these studies suggest determining model order based on cell chemistry and excitation profile, with validation on independent data. The widespread use of the 2RC model as a default appears to be a pragmatic choice for dynamic automotive profiles, rather than an empirically validated optimum.

The OCV is usually modeled by look-up tables, polynomials, combined analytical forms, and splines. The used model influences both identification conditioning and SOC observability, especially for LFP cells with flat OCV. Yu et al. [32] compared 18 OCV models for LFP and NMC cells across various temperatures and aging levels, and found that model suitability depended on cell chemistry and SOC region. Pillai et al. [33], through 28 OCV characterization experiments, demonstrated that widely used polynomial OCV–SOC models introduce substantial errors and quantified the effects of C-rate and cell-to-cell variation. For chemistries exhibiting a flat OCV plateau, such as LFP, minor OCV errors can result in large SOC estimation errors [34]. Consequently, OCV model selection should be regarded as an identification problem in its own right rather than as a preprocessing step. Additionally, the RC parameters vary with temperature, SOC, and aging [8,35], so a single parameter set identified at one operating point seldom describes the entire operating envelope.

2.2. Fractional-Order Models

Electrochemical impedance spectroscopy (EIS) of lithium-ion cells typically exhibits depressed semicircles and low-frequency Warburg-type behavior. Integer-order RC networks can replicate these features only by employing multiple branches. Fractional-order equivalent circuit models (FO-ECMs) address this limitation by replacing capacitors with constant phase elements (CPEs), whose impedance is as follows:

$$Z_{CPE}(s) = {}^{1}/_{(Qs^{\alpha})}, \quad 0 < \alpha \leq 1 \tag{4}$$

where s represents the Laplace variable, Q is the CPE coefficient, and α is the dispersion exponent. If $\alpha = 1$, the CPE behaves like a capacitor, while if $\alpha = 0.5$, it represents a semi-infinite (Warburg) diffusion [7]. This fractional element is approximated in the time domain using the Grünwald–Letnikov (GL) definition as follows:

$$D^{\alpha} x(t_k) \Delta t^{\alpha} = \sum_{j=0}^{L} \omega_j x\left(t_{k-j}\right) \tag{5}$$

$$\omega_j = \left(1 - \frac{\alpha + 1}{j}\right) \omega_{j-1}, \ \omega_0 = 1 \tag{6}$$

where D^{α} is the fractional derivative of order α, x represents the state variable (the CPE voltage in this case), Δt is the sampling time, ω_j are the weights of the GL function, and L is its memory length. Extending this memory allows a single CPE to model slow, distributed diffusion processes. In the implementation case, the sum is truncated to the most recent L samples, in accordance with the short-memory principle [36].

Applying Equation (5) to an ECM with R in parallel with a CPE, where $D^{\alpha}v = -v/(RQ) + i/Q$, produces the updating discrete-time of a fractional-order Kalman filter:

$$v_k = \Delta t^{\alpha}\left(-\frac{v_{k-1}}{RQ} + \frac{i_{k-1}}{Q}\right) - \sum_{j=1}^{L} \omega_j v_{k-j} \tag{7}$$

Equation (7) shows that GL-based FO models incur higher computational costs than integer-order (IO) models because each update requires summing over L previous samples and storing them. Truncating L introduces an approximation error that increases at low frequencies. An alternative in the frequency domain is the Oustaloup recursive approximation [37], which replaces s^{α} within a specified frequency band $[\omega_b, \omega_h]$ with an IO transfer function of order $2N + 1$:

$$s^{\alpha} \approx K\prod_{k=-N}^{N} \frac{s + \omega'_k}{s + \omega_k}, \quad K = \omega_h^{\alpha} \tag{8}$$

$$\omega'_k = \omega_b\left(\frac{\omega_h}{\omega_b}\right)^{\frac{k+N+\frac{1-\alpha}{2}}{2N+1}} \tag{9}$$

$$\omega_k = \omega_b\left(\frac{\omega_h}{\omega_b}\right)^{\frac{k+N+\frac{1+\alpha}{2}}{2N+1}} \tag{10}$$

where ω'_k and ω_k denote the approximation's zeros and poles, and N determines its order.

The CPE impedance described in Equation (4) employs the reciprocal of Equation (8), which consists of a cascade of first-order lag (low-pass) sections. Collectively, these sections replicate the constant phase and the -20α dB/decade magnitude slope characteristic of the CPE within the specified frequency band. Since the resulting system is an ordinary rational transfer function, it can be represented as an integer-order state-space model of fixed size and applied with standard Kalman filters, thereby avoiding the increasing memory requirements associated with Equation (7). However, this approach is accurate only within the frequency range $[\omega_b, \omega_h]$; outside this band, the model exhibits IO system behavior, and modeling wide frequency bands necessitates high orders, which may lead to numerical ill-conditioning. Each approximation has its own trade-offs. The GL method is simple, works directly in discrete time, and is often used for FO state estimation. Its computational cost and accuracy depend on the memory length L. On the other hand, the Oustaloup approximation is less computationally demanding and works well for continuous-time simulation and IO observers, but its accuracy depends on the frequency band and the order N.

Research on FO-ECMs usually shows high impedance fidelity, but the evidence for time-domain benefits is mixed. Wang et al. [8] developed temperature-compensated FO models identified using particle swarm optimization (PSO) and reported mean relative voltage errors below 4% for Li-ion cells under dynamic cycles. Yu et al. [38] introduced a noise-assisted procedure and an information criterion for selecting FO model structures. Tian et al. [39] compared five FO models, and the results show that increased model complexity did not necessarily enhance identification or SOC accuracy. Wang and Liu [40] determined that the FO structure yielded the lowest EIS fitting error among six ECMs. Collectively, these studies support applying CPEs for impedance-based modeling but do not demonstrate a consistent time-domain advantage of FO models over well-identified 2RC

models across different chemistries and profiles. Two practical considerations arise. First, the identified exponents are dependent on the specific approximation used (memory length L and sampling rate for GL, or frequency band and order for Oustaloup), so parameters identified with one implementation may not be transferable to another [39]. Second, additional exponents increase the non-convexity of the identification landscape, which partially explains the prevalence of metaheuristic approaches in FO identification [41,42].

2.3. Electrochemical and Reduced-Order Physical Models

The DFN model [3] and the single-particle model with electrolyte dynamics (SPMe) [4] provide access to internal states, including lithium surface concentration and electrode potentials, which are essential for advanced functions such as plating-aware fast charging [43]. Extensions incorporating double-layer and solid electrolyte interphase (SEI) effects enhance the accuracy of the pseudo-two-dimensional (P2D) model across a broad frequency range (10 mHz to 1 kHz) [44]. However, identification of these models using only full-cell current–voltage data is structurally limited. Bizeray et al. [45] demonstrated that only specific parameter groupings of the single-particle model are identifiable from such data, while additional parameters require half-cell or supplementary measurements. Electrochemical parameter estimation frequently employs metaheuristics; for instance, Li et al. [46] compared 78 metaheuristics on a finite-element P2D model under 5C loading.

2.4. Identifiability, Excitation, and Data

Regardless of the optimizer, the quality of identification is limited by the excitation's information content. Standard protocols include hybrid pulse power characterization (HPPC), dynamic stress test (DST), federal urban driving schedule (FUDS), US06, and worldwide harmonized light vehicle test cycle (WLTC) profiles; low-excitation constant-current data yield highly correlated parameter estimates [20,47]. Optimal experiment design, including reinforcement-learning-based input design [48], is an active approach that moves work away from the optimizer and toward the data. Table 1 summarizes the key characteristics of publicly available datasets that have become community benchmarks, including the MIT-Stanford fast-charging LFP dataset [11], the NASA [49], CALCE [50], and Oxford [14] aging datasets, and the Panasonic 18650PF [51] and KIT NMC [52] drive-cycle and aging datasets.

Table 1. Public benchmark datasets used in the reviewed identification and estimation literature.

Dataset	Chemistry/ Format	Cells	Test Conditions	Temperature	Primary Use/Suitable Tasks	Less Suited for	Ref.
MIT–Stanford–TRI (Severson)	LFP/graphite, 18650	124	Fast-charging protocols; cycled to 80% of nominal capacity	30 °C chamber	Early-life cycle-life prediction; RUL	SOC estimation (no drive cycles); ECM identification (limited pulse data)	[9]
NASA PCoE Battery Data Set	Li-ion, 18650 (2 Ah)	4 per group	CC-CV charge at 1.5 A to 4.2 V, CC discharge at 2 A; EIS; end of life at 30% capacity fade	24 °C and 43 °C groups	Capacity-fade SOH and RUL benchmarking [12,14]	SOC under dynamic loads; cross-cell generalization (few cells)	[49]
Oxford Battery Degradation Dataset	$LiCoO_2$-based, pouch	8	Artemis urban drive-cycle aging with periodic characterization	40 °C	SOH tracking under drive-cycle aging	Population-level prognosis (few cells); temperature generalization	[53]

Table 1. *Cont.*

Dataset	Chemistry/ Format	Cells	Test Conditions	Temperature	Primary Use/Suitable Tasks	Less Suited for	Ref.
KIT NMC/C-SiO aging dataset	NMC/C+SiO, commercial cells	228	Calendar and cyclic aging over a wide range of conditions; capacity and impedance checkpoints; >449 days	Multiple	SOH and aging modeling; impedance-based SOH; evolution of ECM parameters with aging	Real-time SOC estimation (no continuous drive-cycle data)	[52]
CALCE CS2/CX2	$LiCoO_2$, prismatic	≈14 per lot	0.5C CC-CV charge to 4.2 V, 1C CC discharge; full and partial cycling	Room temperature and selected lots at other temperatures	Capacity-fade SOH and RUL	SOC estimation; ECM identification under dynamic loads	[50]
Panasonic 18650PF (Kollmeyer)	NCA, 18650 (2.9 Ah)	1	Drive cycles (US06, HWFET, UDDS, LA92, neural-network cycle) and pulse tests	25 °C down to −20 °C	SOC estimation across temperatures [10]; ECM identification from pulses	SOH and RUL (no aging); cell-to-cell variability	[51]

CC-CV: constant current–constant voltage; EIS: electrochemical impedance spectroscopy; HWFET: highway fuel economy test; UDDS: urban dynamometer driving schedule.

2.5. Implications for Identification and Estimation

The choice of model class determines the dimensionality and conditioning of the identification problem, which in turn influences the selection of an appropriate optimizer. A 1RC model identified using rich pulse data presents a low-dimensional, well-conditioned problem that deterministic least-squares methods can reliably solve. In contrast, a 2RC or FO model identified from drive-cycle data across multiple temperatures is higher-dimensional and exhibits multimodality. Electrochemical models are computationally expensive to evaluate and often include non-identifiable parameter groups. These distinctions are reflected in the comparative evidence presented in Section 3.3 and are further formalized in the decision map in Section 5.2 and the synthesis matrix in Section 5.3.

3. Metaheuristic Optimization for Battery Parameter Identification

3.1. Problem Formulation

As stated in Equation (1), parameter identification is typically defined as the minimization of a voltage-error criterion, subject to box constraints on θ. This is often complemented with penalty terms that ensure physical plausibility (e.g., time-constant separation $\tau_1 < \tau_2$, monotonic *OCV* or with multi-objective formulations that trade voltage precision for parameter smoothness across *SOC*) [54,55] as follows:

$$J(\theta) = \frac{1}{N}\sum_{k=1}^{N}\left[v_{\text{meas}}(k) - v_{\text{model}}(k;\theta)\right]^2 + \lambda P(\theta) \quad (11)$$

$$\theta_{min} \le \theta \le \theta_{max} \quad (12)$$

where N represents the number of samples, $v_{meas}(k)$ is the measured voltage, and $v_{model}(k;\theta)$ is the model's output voltage. The terms θ_{min} and θ_{max} refer to the physical limits of each parameter, this cost function can include also inequality constraints that encode physical knowledge, such as time-constant separation ($\tau_1 - \tau_2 \le 0$) or a monotonic OCV ($-\mathrm{d}OCV/\mathrm{d}SOC \le 0$). λ ($\ge$0) is the optional penalty $P(\theta)$ weight. This penalty function is used for violations of physical plausibility.

Multi-objective formulations balance voltage precision with other objectives, such as parameter smoothness across the SOC [51]. The three most commonly used reporting metrics are root mean square error (RMSE), mean absolute error (MAE), and maximum

absolute error (MaxAE). The RMSE penalizes large deviations, the MAE is less sensitive to outliers, and the MaxAE captures the worst-case scenario, which is particularly relevant for voltage-limit protection. An important but often unstated detail is whether these metrics are computed using the identification data or an independent validation profile; only the latter provides a valid measure of predictive accuracy (Section 6.2).

3.2. Taxonomy of Algorithms

Metaheuristics applied to battery identification are typically categorized according to their underlying metaphor. However, in alignment with the component-based critique in the optimization literature [19,56], this paper organizes them by their principal search mechanism. This approach more clearly highlights the substantive differences among algorithms, as seen in Figure 2.

- Evolutionary algorithms: these algorithms generate new candidates by population recombination and mutation. Genetic algorithm (GA) [57] and differential evolution (DE) [58] are the historical ones and among the early ones used for ECM applications [54,55]. DE variants with adaptive mutation remain competitive baseline algorithms in comparison studies [59].
- Swarm intelligence: these algorithms move candidates according to their own best positions and those of their neighbors. Particle swarm optimization (PSO) [60] is the most cited algorithm in the battery identification literature and frequently ranks among the most accurate and robust options in independent comparisons [61]. Grey wolf optimization (GWO) [62], whale optimization algorithm (WOA) [63], cuckoo search, and salp swarm algorithm [64] have all been applied, with heterogeneous results across studies [65].
- Physics- and mathematics-based methods: Simulated annealing, gravitational search, sine–cosine algorithm (SCA), and gradient-based optimizer (GBO) hybrids exploit non-biological metaphors; several have been benchmarked on Shepherd and ECM models for EV applications [66,67].
- Recent bio-inspired algorithms: the number of new algorithms has increased dramatically over the past five years (snake optimizer [68], honey badger [69], golden jackal [70], bonobo optimizer [71], red-tailed hawk [72], arctic puffin [73], hiking optimization [74], and polar lights optimizers [75]). The majority of these algorithms were published with battery identification as an early application. The field's vigor and fragmentation were demonstrated by a recent representative study that benchmarked twelve untested metaheuristics on 24 datasets covering DST, BJDST, FUDS, and US06 profiles [42]. Variants that use chaotic maps, Lévy flights, or elite opposition-based learning report gradual improvements over their base algorithms [68]. Table 2 synthesizes representative studies from each of these algorithm families, together with their key reported results, and Figure 2 illustrates the taxonomy, with algorithms color-coded by publication era.
- Model-based (surrogate) algorithms: particularly Bayesian optimization (BO), are not considered metaheuristics in the conventional sense. However, they compete directly with metaheuristics when applied to computationally expensive electrochemical models [76,77], and are therefore included in this taxonomy. Hybrid global–local schemes integrate a population-based global search with deterministic local refinement methods, such as the Levenberg–Marquardt (LM) or least-squares approaches [78,79], or decompose the problem into successive stages [40].

This grouping enables the separation of genuine algorithmic contributions from mere relabeling. Mechanisms such as adaptive parameter control [59], opposition-based learning [68], and global–local hybridization [78] can be isolated and evaluated through ablation

studies, whereas introducing a new metaphor alone does not provide any testable property. New algorithms for battery identification should be justified by the mechanisms they introduce and by ablation results, rather than by the novelty of the metaphor.

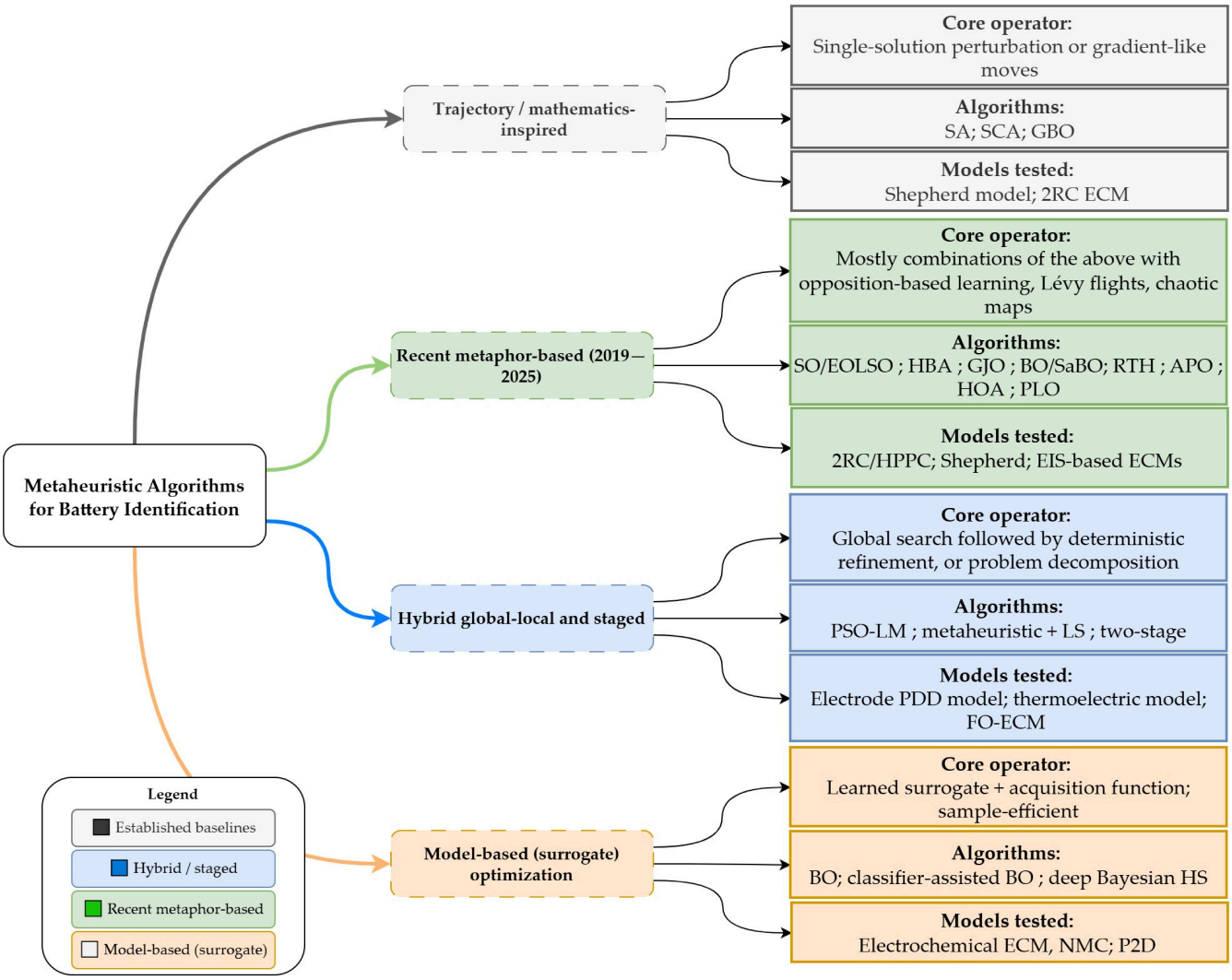


Figure 2. Taxonomy tree of metaheuristic algorithms applied to battery parameter identification.

Table 2. Representative studies of metaheuristic and competing identification methods for battery models. Results are reported as stated by the original authors and are not directly comparable across rows.

Ref.	Family	Methods	Model/Cell/Data	Metric and Result	Statistics	Validation	Evidence
[79]	Mixed (exact, swarm, evolutionary)	9 optimizers, including exact methods, PSO, and firefly	9 ECMs (1RC to 4RC, PNGV and others); whole SOC range	Exact methods best for 1RC at high SOC; PSO best for 2RC; firefly best for 3RC/4RC but slower	Identification time; online performance	SOC comparison	Single study; supports trend 1
[80]	Analytical, least squares, GA, PSO	Three approaches	Dual-polarization (2RC) ECM; two prismatic cells with different anodes; two load profiles	All methods <3% maximum relative voltage error and about 30 mV RMSE in most cases; PSO best trade-off of time, accuracy and robustness	Computational time reported	Two load profiles	Single study; supports trend 1

Table 2. *Cont.*

Ref.	Family	Methods	Model/Cell/Data	Metric and Result	Statistics	Validation	Evidence
[61]	Least squares, PSO, SA, bio-inspired	Traditional vs. metaheuristic	2RC ECM; 12 cells from four public datasets	MSE: bio-inspired methods more accurate than least squares without a significant increase in execution time; PSO most precise and robust	Execution time reported	Four datasets	Single study; supports trend 1
[65]	Swarm, recent	CS, MRFO, JS, GWO, WOA	Randles model; EIS data	CS and MRFO most accurate; success rates of 95% (JS), 85% (GWO) and 65% (WOA)	Repeated runs	NA	Single study; supports trend 2
[46]	78 metaheuristics	78 algorithms	Finite-element P2D model; 5C charge/discharge; simulation; piecewise C-rate validation	TLBO most accurate (moderate cost); algorithms with MAPE < 15% robust; modified TLBO proposed	Accuracy, convergence and robustness compared	Piecewise C-rate profile	Single study; supports trend 2
[40]	Two-stage; 13 bio-inspired algorithms	PSO for structure selection, then 13 algorithms	Six ECMs fitted to EIS data	FO R(RQ)(RQ) model lowest fitting error (MAPE 10.80%); MPA best (MAPE 10.69%)	Friedman ranking test	NA	Single study; supports trends 2 and 3
[68]	Recent	EOLSO vs. GWO, HBA, GJO, ESO, SO	2RC ECM; HPPC data	Relative to SO: SSE −43.83%, MAE −30.73%, RMSE −25.05%	Code released on GitHub	HPPC experiments	Single study; supports trend 2
[66]	Recent	SaBO vs. other optimizers	Shepherd model; EV drive-cycle data	RMSE 8.64×10^{-3}; optimization efficiency 96.6%	Repeated runs	Validation on drive-cycle data	Single study
[67]	Mathematics-inspired	GBO vs. WOA, MVO, SCA, AOA, PSO, RKO, TSA, WSO	Shepherd model; EV application	RMSE 8.64×10^{-3}	NA	NA	Single study
[59]	Evolutionary	DOLADE vs. established algorithms	Battery model for PV energy storage; several discharge experiments	Better than compared algorithms (as reported)	NA	Several discharge tests	Single study
[78]	Hybrid global–local	PSO–LM	2D potential/current-density electrode model	Faster convergence than PSO; avoids LM local minima; good agreement at several C-rates	NA	Several C-rates	Single study; supports trend 3
[48]	Recursive vs. metaheuristic	RLS, EKF, metaheuristics	Four integer-order and three FO models; two OCV test methods	Accuracy, complexity and computational burden compared	Complexity and computational cost	Two OCV tests	Single study; supports trends 2 and 3
[76]	Model-based (BO)	BO vs. gradient descent and PSO	Electrochemical ECM; NMC/graphite cell; experimental drive cycle	Mean testing loss −28.8% vs. gradient descent and −5.8% vs. PSO; variance of testing loss −95.8% and −72.7%	Repeated runs (variance reported)	Drive-cycle verification	Single study; supports trend 4
[77]	Model-based (BO + classifier)	CMABO vs. GA, PSO, SA-TLBO	P2D model; simulation and experiment	More accurate and efficient than compared methods; lower-confidence-bound acquisition best	Acquisition-function choice discussed	Experimental data	Single study; supports trend 4

Table 2. *Cont.*

Ref.	Family	Methods	Model/Cell/Data	Metric and Result	Statistics	Validation	Evidence
[81]	Learning-based (deep Bayesian harmony search)	vs. GA, PSO, LM	Electrochemical model; simulation and experiment	Far fewer model simulations; parameter estimation error about 10 times lower than the second-best method	Number of simulations reported	Experimental data	Single study; supports trend 4

AOA: arithmetic optimization algorithm; CMABO: classification-model-assisted BO; CS: cuckoo search; DOLADE: adaptive DE with dynamic opposite learning; EOLSO: elite opposition-based learning snake optimization; ESO: enhanced snake optimizer; GJO: golden jackal optimizer; HBA: honey badger algorithm; JS: jellyfish search; MPA: marine predators algorithm; MRFO: manta ray foraging optimization; MVO: multi-verse optimizer; PNGV: Partnership for a New Generation of Vehicles model; RKO: red kite optimization; SSE: sum of squared errors; TLBO: teaching–learning-based optimization; TSA: tree-seed algorithm; WSO: white shark optimizer.

3.3. Comparative Evidence

Table 2 summarizes, for representative studies from each family in Figure 2, the model class, cell and data, algorithms compared, evaluation metric and best reported result, evaluation budget and number of runs, statistical tests, and whether validation used independent data. Two aspects of the table are important for interpretation. First, the studies vary in chemistry, profile, and metric, so their numerical results are not directly comparable. Second, budgets, run counts, and statistical tests are often omitted from abstracts and, based on our review, are frequently absent from the full texts as well. This observation is further discussed in Section 6.3.

Observations:

- The advantage of population-based methods over deterministic local methods increases with model order and non-convexity. Lai et al. [79] reported that exact algorithms are ideal for 1RC models across most of the state-of-charge (SOC) range, particle swarm optimization (PSO) is preferable for 2RC models, and the firefly algorithm is most accurate, though slower, for third- and fourth-order models. Kalogiannis et al. [80] found all methods to be adequate for a 2RC model, with maximum relative error below 3%, and identified PSO as offering the best trade-off. Sepúlveda et al. [61] found that bio-inspired methods are more accurate than least-squares for 2RC models of 12 cells and do not take much longer to run. Overall, these results do not show that metaheuristics always outperform local search. Instead, metaheuristics seem most useful when the optimization landscape is complex or when the starting point is not ideal.
- No single algorithm consistently stands out as superior across studies. The top-performing algorithms were CS and MRFO in [65], TLBO among 78 algorithms in [46], MPA among 13 in [40], and EOLSO in [68], with each study using a different model and dataset. This trend aligns with the no-free-lunch (NFL) theorems [82]. The NFL theorems look at performance averaged over all possible problems. While they do not rule out the possibility that one algorithm always performs better within the battery-identification problem class, they show that you must prove such an advantage for that specific class [19]. Another interesting point from individual studies is that two investigations using different optimizers for Shepherd-model identification found the same RMSE (8.64×10^{-3}) [66,67]. This suggests that for low-dimensional models, several algorithms can reach the same best result, but they may differ in how quickly they get there and how much their results vary from run to run.
- Breaking down the model and using hybrid approaches help improve its conditioning. Determining OCV from low-rate or relaxation data before estimating dynamic parameters from pulse or drive-cycle data simplifies the problem and reduces parameter

correlation [42]. Choosing the model structure before searching for parameters has similar benefits [40]. Also, using a global metaheuristic in conjunction with LM or least-squares refinement makes the process more robust to initial values and helps the model converge more quickly [78,83].

- Sample-efficient methods exhibit strong performance when each model evaluation requires substantial computational resources. For instance, in an electrochemical equivalent circuit model (ECM) of a nickel manganese cobalt (NMC) cell, Bayesian optimization (BO) reduced the mean testing loss by 28.8% compared to gradient descent and by 5.8% compared to particle swarm optimization (PSO). Furthermore, BO decreased the variances of the testing losses by 95.8% and 72.7%, respectively [76]. BO's principal advantage over PSO was reliability rather than mean accuracy. Classification-assisted BO [77] and a deep Bayesian harmony-search method [81] achieved higher accuracy with significantly fewer pseudo-two-dimensional (P2D) simulations than genetic algorithms (GA) and PSO. These results indicate that when simulation cost is the primary constraint, sample efficiency becomes more important than the specific characteristics of the search heuristic.

3.4. Fractional-Order Identification

FO-ECM identification adds the CPE exponents to the search space and is now dominated by metaheuristic approaches [41]. Reported results show that FO models identified by hybrid metaheuristics outperform their integer-order counterparts by 20–40% in voltage RMSE on dynamic profiles [38,43], figures that are not directly comparable across studies due to differences in cell chemistries, datasets, and evaluation protocols. Attention must be paid to the interaction between the discretization scheme and the identified exponents: parameters identified with one memory length or sampling rate do not transfer to another, an issue rarely reported but critical for embedded deployment [39].

3.5. Open Challenges for Metaheuristic Identification

The evidence presented indicates that, in most battery identification problems, the primary source of error is not the selection of the optimizer but rather the formulation of the problem, including the informativeness of the data, model structure, constraints, and validation protocol. Six challenges arise from this perspective.

- It is important to consider identifiability before starting optimization. If two parameters affect the voltage only through their product or ratio, as seen in some SPM parameter groups [45], no optimizer can tell them apart. A metaheuristic will find just one of many possible solutions, and repeated runs will spread the results along a ridge in the cost function. Before claiming accurate identification, it is best to perform a sensitivity or Fisher information analysis or at least report how much the identified parameters vary across repeated runs. Often, improving experimental design is more helpful than creating a new optimizer [47,48].
- Parameters need to be generalizable. If you calibrate a parameter set using only one profile at one temperature, it will describe only that specific case and will not give you a full cell model. To validate your parameter identification, use different profiles and, when possible, test at various temperatures and aging states. For parameters that change with SOC or temperature, use functions or look-up tables with smooth transitions [55].
- Ensuring physical plausibility is essential. Excessively broad box constraints can allow compensating parameter errors. Implementing physical inequality constraints and penalties (Equation (7)) reduces this risk. For safety-critical applications, internal-state checks are required (Section 6.5).

- Online implementation requires a specific trade-off. Although most metaheuristic identification occurs offline, recursive least squares (RLS) and Kalman filter-based estimators track slowly varying parameters more effectively online. Comparative studies demonstrate that these methods surpass particle swarm optimization (PSO) in accuracy, robustness, and computational cost [84]. An effective system architecture utilizes a metaheuristic offline or in the cloud to initialize parameters and bounds, while a recursive estimator onboard monitors parameter evolution.
- Demonstration of novelty should focus on the underlying mechanism. Algorithmic variants incorporating chaotic maps, Lévy flights, or opposition-based learning have reported improvements over their base algorithms [68]. However, these improvements are only meaningful when evaluated against robust baselines and through ablation studies of the added mechanisms [19,85].

4. Artificial Intelligence for Battery State Estimation

4.1. From Model-Based Observers to Data-Driven Estimators

Classical SOC estimation includes an ECM and a state observer, such as an extended or unscented Kalman filter (EKF/UKF), a sliding-mode observer, an H-infinity observer, or a particle filter [2,34]. These remain the industry standard: they are lightweight, interpretable, and have analyzable error dynamics. Their accuracy, however, is limited by model fidelity and the quality of noise-covariance tuning [86,87], which is typically handled by metaheuristics [41]. Under laboratory dynamic profiles, adaptive EKF formulations using higher-order ECMs report SOC errors below 1% [5]. Point accuracies, such as fractional-order comparisons in Section 3.4, are useful indicators of achievable performance; nevertheless, they are not directly comparable across investigations due to changes in chemistry, temperature, and excitation patterns.

Chemali et al. [10] demonstrated that a single LSTM can map current, voltage, and temperature sequences directly to SOC across temperatures, achieving an MAE of 0.573% at a fixed ambient temperature and 1.606% on a dataset with ambient temperature increasing from 10 to 25 °C (Panasonic 18650PF NCA cell; single study). Yang et al. [11] trained a stacked LSTM network on LFP cells using DST, US06, and FUDS profiles. They reported an RMSE within 2% and MAE within 1%, even when the initial SOC was inaccurate. The model outperformed a UKF and achieved sub-millisecond computation per time step on a desktop computer. Severson et al. [9] predicted the cycle life of 124 commercial LFP/graphite cells using data from the first 100 cycles, achieving a 9.1% test error. They also classified cells into short- and long-lived groups based on the first five cycles, with a test error of 4.9%. For SoH estimation, feature-based machine learning was compared (incremental capacity analysis features, charge-curve statistics, and impedance features) against end-to-end deep learning on raw partial charge curves [14,24,27].

4.2. Deep Architectures

Recurrent networks, particularly LSTM and GRU architectures, are the most widely used models for mapping measurement sequences to states. Their accuracy on laboratory drive cycles typically falls within the 1–2% state-of-charge (SOC) range at fixed temperature, but performance declines as temperature varies; this trend is corroborated by several studies [10–13]. Guo and Ma [88] compared a fully connected network, LSTM, GRU, and a TCN on two cell types and found that the three sequence models outperformed the fully connected network. Among these, the TCN demonstrated the greatest robustness to temperature fluctuations and noise, while the GRU exhibited the shortest per-step computation time. Naguib et al. [89] reported similar findings regarding the accuracy of GRU, LSTM, and TCN networks for SOC estimation. Convolutional networks and TCNs leverage local

patterns in charge curves and enable greater parallel computation. Simpler architectures may also suffice: on NASA cells B0005–B0007, a multilayer perceptron achieved an SOH RMSE of 0.0069 on B0005, whereas GRU and LSTM networks required longer training without improving accuracy [12]. This outcome likely reflects the small, homogeneous nature of such datasets rather than indicating a general superiority of shallow networks.

Attention-based and Transformer models can capture long-range dependencies and facilitate transfer across different cells. A self-supervised Transformer achieved an SOC RMSE of 0.90% and an MAE of 0.44% under constant-temperature conditions, and an RMSE of 1.19% under varying-temperature conditions. With self-supervised pre-training, the model achieved an RMSE of less than 1.9% using only 20% of the training data, and its learned weights were successfully transferred to a cell with different chemistry [13]. However, these advantages are accompanied by increased data requirements and attention costs that scale quadratically with sequence length [25].

Probabilistic methods like GPR [14] and Bayesian neural networks with Monte Carlo dropout [90] provide uncertainty estimates for safety-critical BMS functions. In contrast, deterministic deep networks do not offer these estimates. Ke et al. [90] tested their Bayesian pipeline on four datasets, which included regular charging, fast charging, and second-use applications.

Transfer learning [91] and weakly supervised learning with imprecise interval labels [92] mitigate the scarcity of labeled state-of-health (SOH) data and facilitate adaptation to diverse cell types and operating conditions. Table 3 summarizes representative studies of these architectural classes, detailing their data, validation protocols, and reported results. Figure 3 positions these classes in relation to data requirements and physical structure.

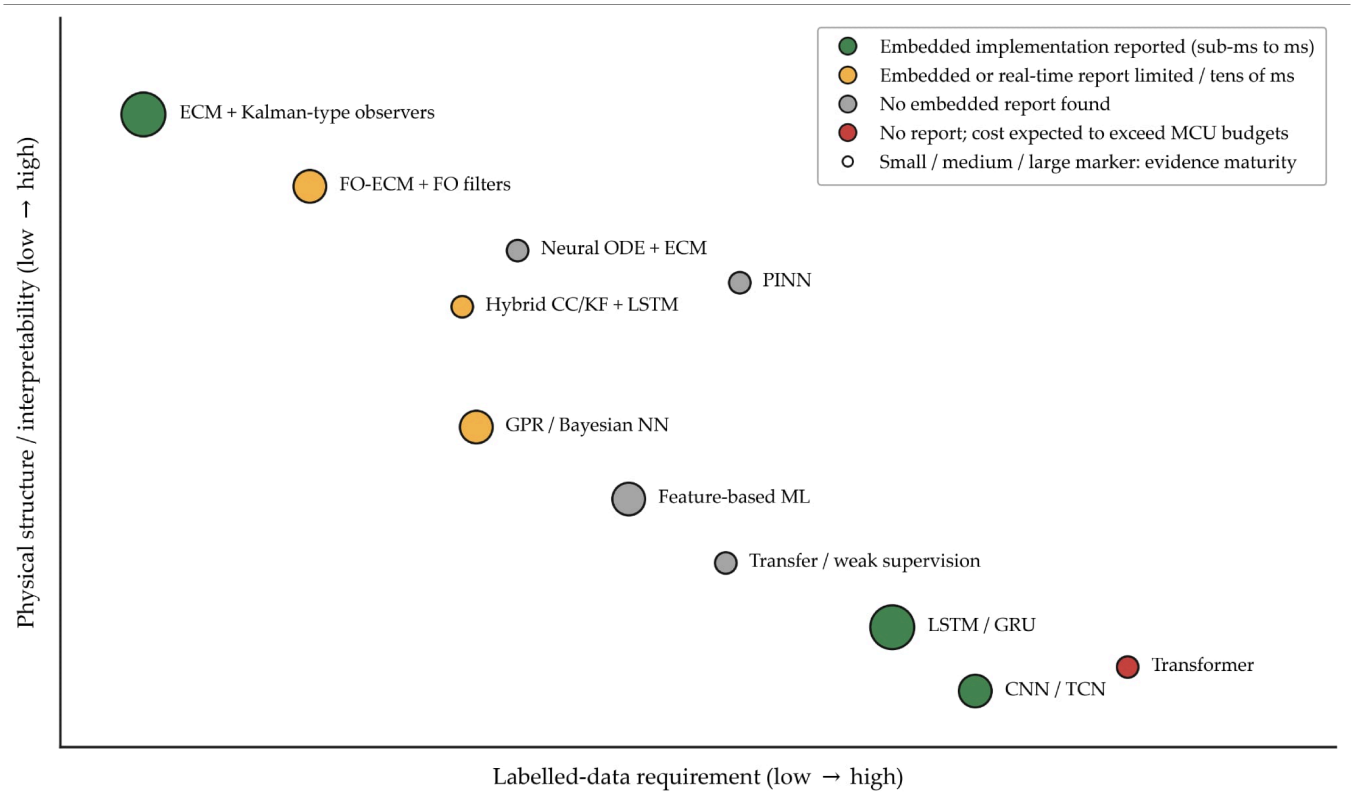


Figure 3. Qualitative positioning of SOC/SOH estimator classes is presented according to labeled-data requirements (horizontal axis) and the degree of embedded physical structure and interpretability (vertical axis). Marker color represents embedded, while marker size reflects the maturity of the evidence base.

Table 3. Synthesis of AI architectures applied to SOC/SOH estimation.

Ref.	Architecture	Target	Cell/Dataset	Conditions and Validation	Reported Result	Uncertainty	Cost/ Hardware Reported	Evidence Type
[10]	LSTM	SOC	NCA 18650 (Panasonic 18650PF)	Drive cycles; fixed and varying temperature	MAE 0.573% at fixed T; 1.606% with T rising 10 → 25 °C	No	Not reported	Single study
[11]	Stacked LSTM	SOC	LFP cells	DST, US06, FUDS; training and testing on different profiles; unknown initial SOC	RMSE within 2%; MAE within 1%; better than UKF	No	Sub-millisecond per step (desktop)	Single study
[88]	FCNN, LSTM, GRU, TCN	SOC	Two cell types; dynamic drive cycles	25 °C accuracy; robustness to temperature and noise; cross-chemistry test	Sequence models more accurate than FCNN; TCN most robust	No	GRU shortest time per step	Single study
[13]	Self-supervised Transformer	SOC	Li-ion cells; transfer to a different chemistry	Constant and varying temperature; reduced training data	RMSE 0.90%, MAE 0.44% (constant T); RMSE 1.19% (varying T)	No	GRU shortest time per step	Single study
[9]	Feature-based regularized regression	Cycle life	124 LFP/graphite cells (MIT–Stanford–TRI)	Held-out test cells	9.1% test error (first 100 cycles); 4.9% classification error (first 5 cycles)	No	Not reported	Single study
[14]	GPR	SOH/RUL	Capacity-versus-cycle data from Li-ion cells	Short- and long-term forecasting	Predictive intervals reported	Yes (native)	Not reported	Single study
[90]	Bayesian neural network (MC dropout)	SOH	Four datasets (regular charging, fast charging, second use)	Automatic feature selection (RFECV)	Superior to compared DL methods (as reported)	Yes	Not reported	Single study
[12]	MLP, GRU, LSTM, TCN	SOH	NASA B0005–B0007	Per-cell evaluation	MLP RMSE 0.0069 (B0005)	No	GRU/LSTM longer training	Single study
[93]	Uncertainty-weighted PINN	SOH	Real-world EV operating data	IC-curve-based SOH labels; driving-behavior features	MAPE 2.69%; RMSPE 2.96%	Variance weighting	Low computational cost (as reported)	Single study
[16]	Neural ODE and RNN	SOH	Battery SOH trajectories from capacity and charge-voltage profiles	Multi-battery learning; longer prediction windows; SOH RMSE and EOL tracked	ODE-based and PC-RNN models outperformed LSTM/GRU in >80% of experiments; ~1% SOH error at 70% life; ~4% at 20% life; 5% EOL error when predicting 30% remaining life	Not reported	Not reported	Single study
[91]	Deep transfer learning	SOC and SOH	Not specified in attached table	Cross-domain transfer	Quantitative result not given in attached table	Not specified in attached table	NA	Single study
[92]	Weakly supervised learning	SOH	EV operating conditions	Imprecise-interval labels; physical rationality correction	High accuracy across interval widths (as reported)	Interval labels	NA	Single study

Table 3. *Cont.*

Ref.	Architecture	Target	Cell/Dataset	Conditions and Validation	Reported Result	Uncertainty	Cost/ Hardware Reported	Evidence Type
[86]	Hierarchical adaptive EKF (model-based)	SOC	Not specified in attached table	Laboratory dynamic profiles	SOC error below 1%	Filter covariance	NA—	Single study
[94]	PSO-tuned LSTM	SOC	Not specified in attached table	Different operating conditions; input noise	Error within 0.5%	No	NA	Single study (interface I1)

FCNN: fully connected neural network; IC: incremental capacity; MC: Monte Carlo; MLP: multilayer perceptron; RFECV: recursive feature elimination with cross validation; RMSPE: root mean square percentage error. Embedded implementations are summarized separately in Section 7.2.

4.3. Hybrid Physics-Informed Approaches

Outside the training distribution, where safety is paramount, purely data-driven estimators perform poorly. Hybrid techniques are considered the most promising current direction, since they include physical structure in the learning problem:

- Physics-informed neural networks (PINNs): the loss function enforces the governing equations (diffusion PDEs, ECM state equations) as soft constraints [93]. Compared with purely data-driven methods, SOH estimation applied to real-world EV data is more robust to distribution shifts [93].
- Neural ODEs and hybrid state-space models: While neural networks learn residual dynamics, parameter dependencies on SOC/temperature, or unmodeled aging effects [16,17], neural ODEs [16] learn continuous-time dynamics and readily integrate with circuit models. The backbone is provided by the established ECM structure. This reasoning is extended to CPE dynamics by fractional-order neural ODE hybrids. Compared with end-to-end networks, these architectures offer irregular sampling, maintain state interpretability (the SOC remains a physical state), and require less data.
- Digital twins: battery digital twins for fleets are built at the system level using ECM/electrochemical backbones in conjunction with recurrent or neural-ODE correctors that are constantly re-identified from telemetry; early tests on multi-vehicle EV telemetry demonstrate that SOH can be tracked from field data without specific characterization tests [27,41].

4.4. From Laboratory to Field Data

The discrepancy between field circumstances and laboratory benchmarks is a recurrent finding in recent surveys [41]. Partial, erratic charge events, clock drift, sensor noise, variations in ambient temperature, and a lack of ground-truth capacity are all present in field data. In field telemetry, methods that top laboratory leaderboards often deteriorate dramatically. Fleet-level hierarchical models, physics-informed regularization, and weak supervision from opportunistic full charges are examples of practical advancements [92,93]. For upcoming SOH literature, we consider field data validation an essential component of reporting.

4.5. Open Challenges for AI-Based Estimation

SOC errors of 1–2% on laboratory drive cycles are now routinely reported (Table 3). The primary factors limiting the usefulness of AI estimators are generalization, calibration, and cost, rather than the choice of architecture. Six key challenges are discussed below.

Generalization is often evaluated too narrowly. Random train/test splits that include cycles from the same cell in both sets, or that use identical temperature and profile conditions for training and testing, tend to overstate accuracy [23,25]. More rigorous approaches are

necessary, such as cell-wise (leave-one-cell-out), cross-temperature, cross-profile, and, where applicable, cross-chemistry splits. The transfer results presented in [13,91] illustrate effective reporting of such tests.

Ground-truth data are limited in real-world applications. Laboratory SOH labels are derived from reference capacity tests, which are seldom available in vehicles. Interval-valued labels [92], incremental-capacity-derived labels [93], and physics-based priors partially address this limitation. However, these approaches make the reported error dependent on the label definition, which must therefore be explicitly stated.

Uncertainty is rarely quantified or calibrated. Only a minority of the studies in Table 4 report uncertainty, and fewer still test whether the predicted intervals are calibrated [14,90]. For BMS functions that trigger protective actions, an uncalibrated point estimate is of limited use.

Cost is rarely assessed. Accuracy is typically reported using offline, double-precision computations on desktop hardware. Section 6.4 shows that small recurrent networks can operate within microcontroller budgets, but quantization may affect accuracy rankings. Architectures should be compared at deployment precision.

Physics consistency is only partially enforced. In PINNs, physical residuals are included in the loss function with adjustable weights, so physical consistency is encouraged but not guaranteed. The weight setting is also a hyperparameter. Ablation studies that toggle physics terms, as in [93], should become standard practice.

Metrics can be misleading. Errors averaged over the full SOC range are dominated by the flat OCV region for LFP, and sensitivity to the initial SOC is often untested [11]. Reporting errors by SOC region, MaxAE, and convergence from incorrect initial states provides a more accurate assessment.

Table 4. Synthesis matrix relating model and estimator classes to identification approaches, BMS targets and practical attributes.

Class	Identification Approach	BMS Targets	Computational Complexity	Interpretability	Online Suitability	Data Requirement	Uncertainty	Chemistry Transferability	Embedded Feasibility	Key Refs.
Rint/1RC ECM	LS, RLS, EKF	SOC, SOP	Very low	High	High	Low (pulse/HPPC)	Via filter covariance	Structure transfers; re-parameterization needed (add hysteresis for LFP)	High	[6,31,84]
2RC/nRC ECM	LS/LM offline; PSO/DE for multi-temperature or poorly initialized problems; RLS online	SOC, SOP, voltage prediction	Low	High	High	Low–moderate (HPPC + drive cycles)	Via filter covariance	Structure transfers; order is chemistry dependent	High (sub-ms EKF on automotive MCU)	[79,80]
FO-ECM	Metaheuristic (+local refinement) offline; FO-KF online	SOC; impedance-based SOH	Moderate (grows with memory length L)	Moderate–high (CPE related to diffusion)	Moderate (truncation trade-off)	Moderate (EIS + time-domain data)	Via FO filters	Moderate	Moderate	[8,39,40]
SPM/SPMe	Staged identification (OCV, then kinetics); BO or metaheuristic	Internal states, fast-charge constraints, SOC	Moderate–high	High (physical states)	Moderate (reduced-order observers)	High (multi-rate, half-cell data)	Observer-based	Structure transfers; parameters do not	Low–moderate	[4,45]
DFN/P2D	BO; surrogate-assisted metaheuristics	Design, plating-aware fast-charge optimization, offline diagnosis	Very high	High	Low	Very high	Limited (rarely posterior estimates)	Structure transfers; parameters do not	Low (offline or cloud)	[3,46,76,77]
Data-driven DL (LSTM, GRU, CNN/TCN, Transformer)	Gradient training; metaheuristic or BO hyperparameter tuning	SOC, SOH, RUL	Moderate (inference); high (training, Transformers)	Low	High for small RNN/CNN; lower for Transformers	High (labeled data across temperature and aging)	Only with ensembles or Bayesian layers	Low without transfer learning	Moderate (small INT8 models on MCUs)	[10,13,88]

Table 4. *Cont.*

Class	Identification Approach	BMS Targets	Computational Complexity	Interpretability	Online Suitability	Data Requirement	Uncertainty	Chemistry Transferability	Embedded Feasibility	Key Refs.
Probabilistic ML (GPR, BNN)	Bayesian inference; MC dropout	SOH, RUL	Moderate (GPR training scales cubically with data)	Moderate	Moderate (periodic updates)	Low–moderate	High (native)	Moderate (priors, multi-output GPs)	Low–moderate	[14,90]
Physics-informed hybrids (PINN, neural ODE + ECM)	Gradient training with physics loss; ECM backbone by LS or metaheuristic	SOH, SOC, parameter adaptation	Moderate–high	Moderate–high	Emerging	Moderate (reported lower than pure DL; limited evidence)	Possible (uncertainty-weighted losses)	Promising but under-validated	Emerging (few embedded reports)	[16,93]

BNN: Bayesian neural network; KF: Kalman filter; LS: least squares; MCU: microcontroller unit; SOP: state of power.

5. Synergies: Metaheuristics Meet Machine Learning

5.1. Interfaces Between Metaheuristics and AI

The two methodological families interact and compensate for each other's shortcomings; therefore, the convergence of metaheuristic optimization and artificial intelligence is not merely a coincidence. These synergies are divided into four main interfaces:

i. Metaheuristic hyperparameter and architecture optimization: learning rates and architecture size have a significant impact on SOC/SOH network performance. GA or PSO variations are frequently used to adjust parameters, including learning-rate schedules, layer sizes, window lengths, and regularization weights. PSO-tuned LSTM, for example, reported SOC errors within 0.5% [94]. Comparative research, however, shows that Bayesian optimization and grid search remain robust baselines that metaheuristic publications should include in their assessments (but frequently neglect to do so) [18,26].

ii. Metaheuristic training of small networks: Metaheuristics can completely replace gradient descent for shallow estimators (such as ELM, RBF, and ANFIS). In small, extremely non-convex optimization problems, this method successfully avoids suboptimal local minima [26]. This is feasible only for small parameter counts; for deep networks, gradient training remains far more efficient.

iii. Learned surrogates inside identification loops: the DFN model and other electrochemical simulators are computationally expensive. Kim et al. integrated a GA with a one-dimensional convolutional network to learn the current–voltage dynamics of a pseudo-two-dimensional (P2D) model, thereby proposing candidate parameters [95]. Additionally, a deep Bayesian neural network reduced the number of required electrochemical model simulations compared with GA, PSO, and Levenberg–Marquardt (LM) methods [81]. Furthermore, a classifier that rejects parameter vectors likely to cause P2D model convergence failure enhanced the efficiency of BO [77]. BO functions as a surrogate method, utilizing a Gaussian process as the learned model [76].

iv. Optimization of the estimation pipeline: Metaheuristics are often used to optimize the larger estimation framework beyond training. This involves determining the OCV model structure [32], selecting the best features for SOH regressors [90], and adjusting filter covariances [83,87].

Figure 4 depicts these four interfaces as a closed-loop synergy diagram.

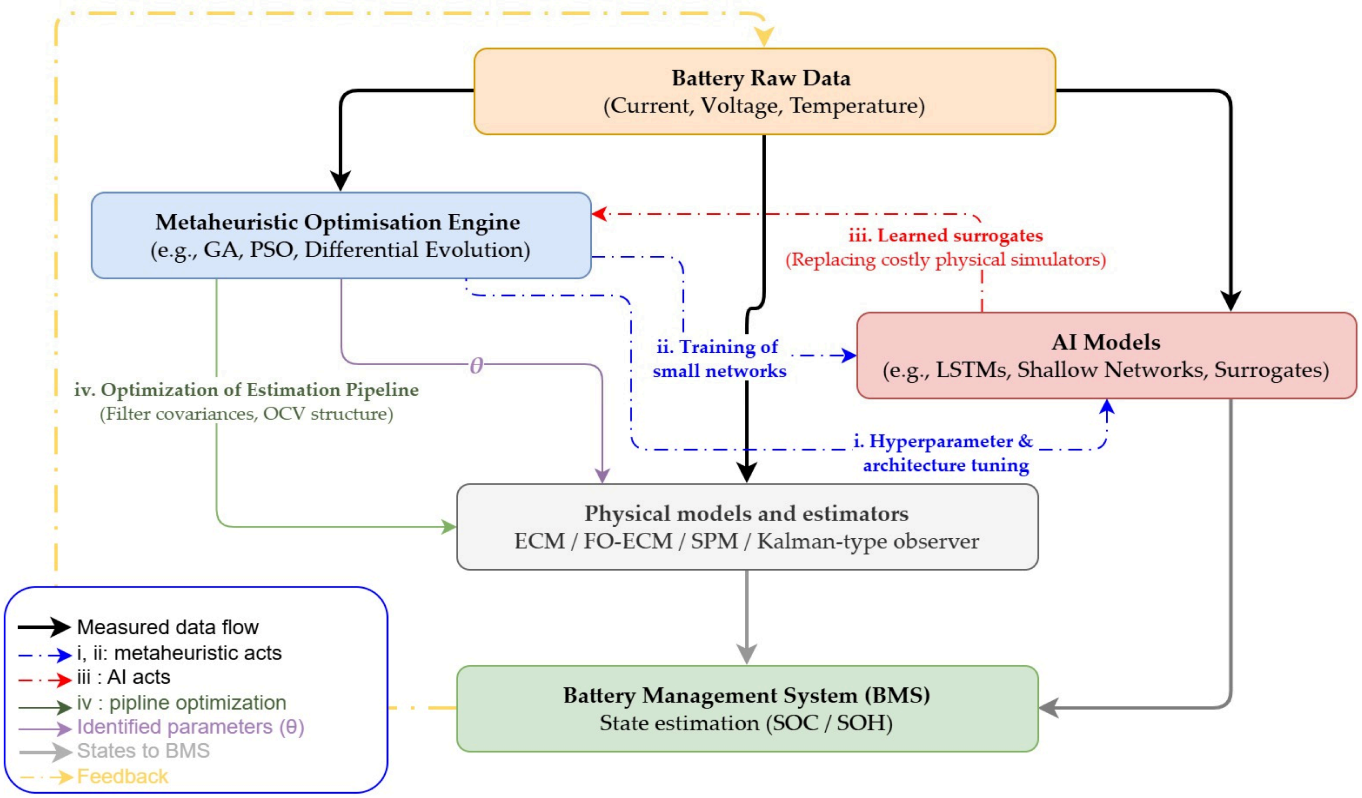


Figure 4. Interaction diagram between metaheuristic optimization and AI models across the BMS pipeline.

5.2. When Is Metaheuristic Identification Warranted?

The trends identified in Section 3.3 can be formalized into a decision rule based on three key properties: the cost of a single model evaluation, the dimensionality and multimodality of the optimization landscape, and the requirement for online parameter tracking, as illustrated in Figure 5.

If parameters are not identifiable from the available data, optimization is ineffective, and modifications to the experiment or model parameterization are necessary [45,47]. For low-order ECMs with informative pulse data identified offline, deterministic least-squares or LM methods are sufficient and cost effective [79,80]. For online tracking of slowly varying parameters, recursive estimators such as recursive least squares (RLS) or EKF are preferred [42,84]. For higher-order, fractional-order (FO), or multi-temperature ECMs, where evaluation is inexpensive but the landscape is multimodal, population-based methods are recommended such as PSO, DE, or covariance matrix adaptation evolution strategy (CMA-ES), ideally followed by local refinement [78,79]. The specific algorithm should be selected through benchmarking rather than novelty (Section 6.1). When each evaluation is costly, as in P2D or DFN models, BO and surrogate-assisted searches are preferred, with population-based methods considered only under equivalent and limited computational budgets [76,77,81].

5.3. Matching Model Classes and AI Architectures to BMS Tasks

Table 4 synthesizes the evidence from Sections 2–4 and 6.4 into a matrix that relates each model or estimator class to its typical identification approach, primary BMS targets, and nine practical attributes. The entries represent a qualitative assessment, supported by the references in the last column, and are intended as a starting point for method selection rather than a ranking.

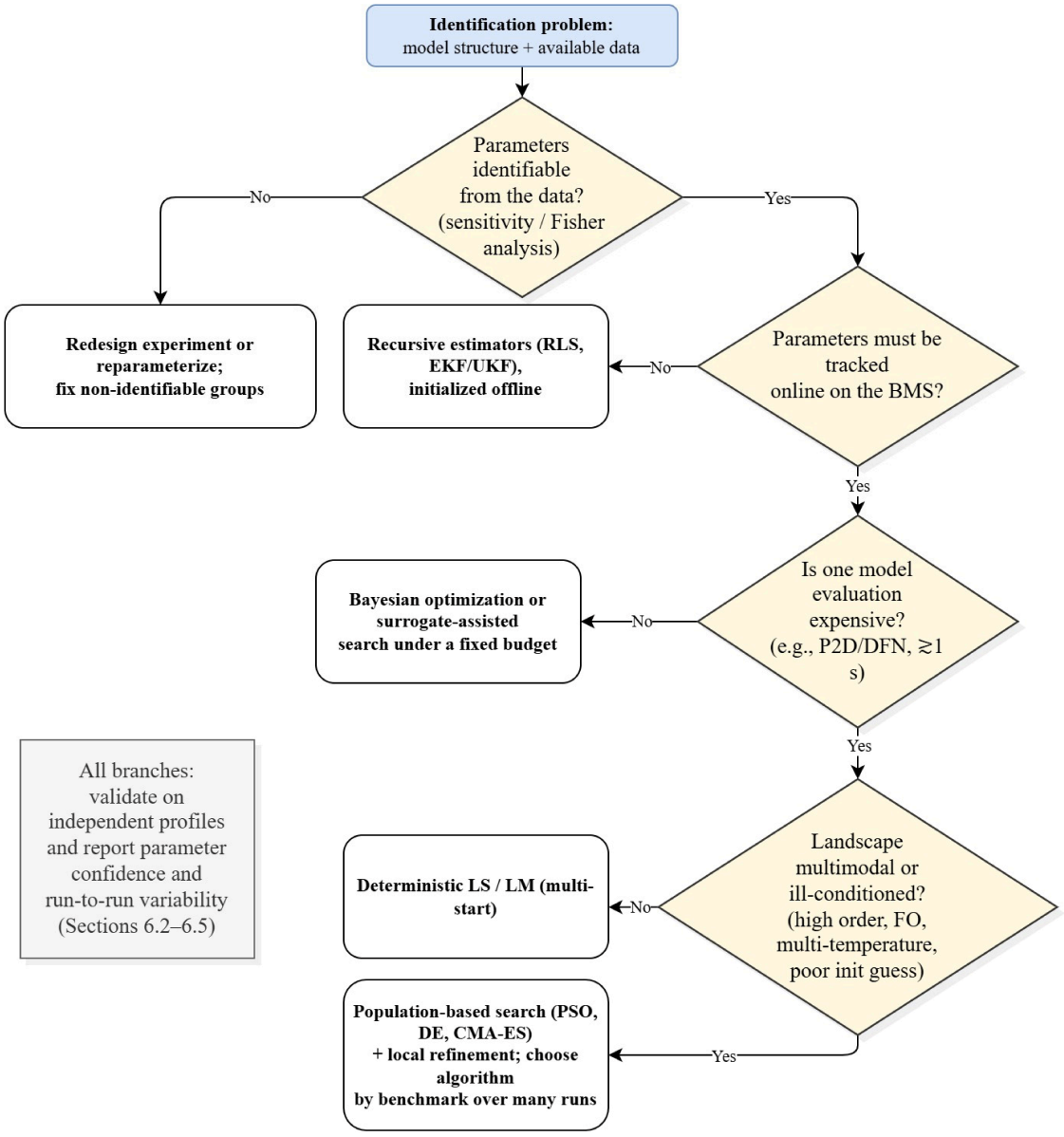


Figure 5. Decision map for selecting an identification approach.

Table 4 reveals three notable patterns. First, attributes are traded off along the rows; no class simultaneously achieves low data requirement, high interpretability, native uncertainty, and high embedded feasibility. Second, ECM classes are the only ones with strong evidence of embedded feasibility combined with high interpretability, which accounts for their prevalence in production BMSs. Third, hybrid classes offer the most favorable combination of attributes, although their transferability and embedded feasibility are supported by limited studies.

5.4. Where Do Physics-Informed Hybrids Add Measurable Value?

Current evidence indicates that hybrid approaches provide measurable value in three scenarios: when labels are scarce and physical structure must substitute for data, as observed in field SOH estimation with weak labels [92,93]; when estimates must remain physically interpretable, such as SOC represented as a state of an ECM corrected by a learned residual [16]; and when extrapolation beyond the training conditions is necessary. Embedded implementation is also feasible. For example, a hybrid combining Coulomb counting and a one-layer LSTM network (hidden size 10) via a Kalman filter required 21 ms and 5444 bytes of

RAM per step on a 16 MHz 8-bit ATmega2560 processor [96]. However, three aspects have not yet been convincingly demonstrated: transferability across chemistries, calibrated uncertainty, and validation on large fleets with reference capacity measurements. The benefits of the added complexity should therefore be demonstrated on a case-by-case basis, using ablation studies against both the physics-only and data-only components.

6. Critical Discussion

Although battery state estimation has undoubtedly been improved by metaheuristic and AI techniques, the literature contains several systemic methodological flaws. The main problems found in this review are listed in Table 5 along with recommended solutions.

Table 5. Methodological pitfalls in battery parameter identification and state estimation, alongside proposed best practices.

Pitfall	Domain	Consequence	Proposed Best Practice	Evidence
Novel-Algorithm Inflation	Metaheuristics	Spurious assertions of universal supremacy and the proliferation of algorithms that differ only in metaphor.	Benchmark against highly tuned conventional algorithms (e.g., PSO, DE); acknowledge the no-free-lunch theorem.	Different "best" algorithms across studies (Table 3, trend 2); component analyses [19]
In-Sample Evaluation	Both	Overfitting refers to models that achieve high accuracy on training data but fail to generalize.	Maintain a strict separation between training/identification datasets and testing/validation profiles.	Many studies identify and evaluate on the same profile; random splits leak cycles from the same cell [25]
Absence of Statistical Testing	Metaheuristics	Single-run results conceal the variability and reliability of stochastic algorithms.	Mandate the reporting of variation, mean, and worst-case performance over several independent runs.	Budgets, run counts and tests missing in many rows of Table 3
Neglecting Embedded Feasibility	Both	High-accuracy algorithms remain theoretical due to microcontroller memory/time constraints.	Provide the inference time, memory use, and reduced-precision arithmetic performance.	Few studies report execution time or memory (Section 7.2)
Output-Error Overreliance	Both	Voltage RMSE minimization can result in physically impossible internal parameters.	Validate internal states against reference measurements or set strong physical constraints during optimization.	Good voltage fit with out-of-range parameters [84]; identifiability limits [43]

6.1. Novel-Algorithm Inflation

Hundreds of nature-inspired algorithms have been developed, many of which differ from known approaches simply in metaphor [18]. The metaheuristic literature is growing at a rate that is unrelated to methodological advancement. Battery parameter identification is a common initial application because it is a practical nonlinear testbed. According to the no-free-lunch theorem [82], performance on the particular problem class is what matters, as shown against strongly tuned baselines (PSO, DE, CMA-ES, Bayesian optimization) and validated by statistical testing over numerous independent runs. Claimed universal superiority is implied to be meaningless. These requirements are only met by a small percentage of the surveyed research [42,54].

6.2. In-Sample Evaluation and Data Leakage

Across the identification literature, recurring deficiencies are identified as follows:

- Inconsistent datasets and profiles that prevent cross-study comparison;
- Single-run results without variance reporting;
- Unequal function-evaluation budgets across compared algorithms;
- Lack of code and identified-parameter release;
- In-sample evaluation: parameters are fitted and evaluated on the same profile.

The AI estimation literature has similar issues: random train/test splits that leak cycles from the same cell, metric selection that favors flat areas of the SOC range, and the lack of cross-chemistry evaluation [23,25]. Community benchmarks with fixed splits, inspired by computer-vision leaderboards, are overdue.

6.3. Absence of Statistical Testing

Metaheuristics are inherently stochastic, so a single run provides limited information about expected performance. However, the identification literature frequently reports single-run results without variance estimates, compares algorithms with unequal numbers of function evaluations, and omits the code and identified parameters (Table 2). Comparative studies should use equal evaluation budgets, report the mean, standard deviation, and worst-case performance over multiple independent runs (30 is a common choice), apply non-parametric tests such as the Wilcoxon signed-rank test for pairs and the Friedman test with post hoc correction for multiple algorithms, as demonstrated in [40], and release code and identified parameters, as in [68]. Community benchmarks with fixed data splits and evaluation budgets, analogous to computer vision leaderboards, are needed (Section 7.3).

6.4. Embedded Feasibility

Reported accuracy is typically obtained offline using double-precision floating-point on desktop hardware. Embedded BMS implementation requires fixed-point or reduced-precision arithmetic, kilobyte-scale memory, millisecond-scale deadlines, and functional-safety requirements according to the international standard for the functional safety of electrical and electronic systems (ISO 26262). Fractional operators with extended memory, transformer inference, and particle filters can all exceed these budgets. Few papers report inference time, memory footprint, or quantization robustness; those that do show order-of-magnitude differences amongst algorithmic families [11]. We believe that hardware-aware assessment should become commonplace. Table 6 collects the studies in our sample that report hardware-level measurements.

Table 6. Summary of studies reporting hardware-level power and performance measurements.

Ref	Estimator(s)	Processor/ Platform	Precision/ Toolchain	Execution Time	Memory	Accuracy Reported
[97]	EKF, EKF-RLS, FNN, LSTM	Two NXP S32K microprocessors (processor-in-the-loop)	Automatically generated code	0.24, 0.25, 0.14 and 0.71 ms (faster processor)	Neural estimators < 1 kB RAM per instance, lower than the EKFs	<5% maximum SOC error for all four
[98]	Coulomb counting + 1-layer LSTM (hidden size 10) fused by a Kalman filter	ATmega2560, 16 MHz, 8-bit	Embedded C	21 ms per step	5444 bytes RAM	Hybrid SOC estimation

Table 6. *Cont.*

Ref	Estimator(s)	Processor/ Platform	Precision/ Toolchain	Execution Time	Memory	Accuracy Reported
[96]	CNN, LSTM, CNN-LSTM, TinyCNN	ESP32	TensorFlow Lite Micro; post-training INT8 quantization	TinyCNN 41.99 ms mean latency	TinyCNN 2913 parameters, 8.51 KiB (INT8)	US06: best FP32 MAE 1.31% (CNN-LSTM); best INT8 MAE 1.70% (LSTM); TinyCNN INT8 MAE 2.55%
[99]	GPR + surrogate-optimized LSTM	STM32F411RE (Nucleo)	MATLAB/Simulink code generation	1.108 ms per sample	—	RMSE 0.74% (constant-current discharge, 2–3 A only)

FNN: feedforward neural network; FP32: 32-bit floating point; INT8: 8-bit integer.

Four conclusions can be drawn from Table 6:

- Small recurrent and feedforward networks are compatible with microcontroller resource constraints: on an automotive-grade processor, an LSTM step required 0.71 ms, and the neural estimators used less than 1 kB of RAM per instance, which is less than the requirement for EKFs [97].
- Execution time varies by approximately two orders of magnitude across platforms, ranging from sub-millisecond on 32-bit automotive processors to tens of milliseconds on an 8-bit device [96] or when using an interpreted INT8 runtime [98]. Therefore, latency claims are meaningful only when the processor and network sizes are specified.
- Quantization can alter the ranking of architectures; for instance, in [98], the most accurate FP32 model (CNN-LSTM) was not the most accurate INT8 model (LSTM).
- Pack-level deployment increases the computational cost in proportion to the number of estimator instances, as explicitly evaluated in [97]. The scope of validation is also significant; for example, ref. [99] was validated exclusively on constant-current discharge. Consequently, hardware-aware evaluation should be adopted as standard practice.

6.5. Physical Plausibility Versus Fit Quality

Both metaheuristic identification and AI estimation enhance output-error criteria. However, a low RMSE does not guarantee accurate internal behavior: output-error tests pass even with compensating parameter errors, sign-inverted temperature dependence, and unphysical CPE exponents. For safety-critical applications, such as fast-charging control with anode-potential limitations, validation must include internal-state checks against reference measurements (e.g., three-electrode cells, EIS) or, at the very least, plausibility constraints within the identification itself [43,45].

7. Future Research Directions

7.1. Chemistry Transfer and Emerging Chemistries

The majority of existing identification processes and AI estimators have been validated primarily using LFP and NMC chemistry. As the market evolves, these methodologies must be rigorously reassessed for silicon-blended anodes and developing sodium-ion cells. Sodium-ion cells built on hard-carbon anodes exhibit a markedly different OCV–SOC signature from graphite-based Li-ion cells: a low-slope, quasi-plateau region combined with pronounced voltage hysteresis linked to the disordered pore structure of hard carbon, along with distinct impedance and aging mechanisms; existing lithium-ion modeling and state-estimation techniques can be partially transferred but require substantial reparameterization and, in several cases, new model structures [28]. Creating transferable

OCV representations and using meta-learning to initialize parameter identification across different cell types are extremely intriguing directions for future research.

7.2. Sodium-Ion Batteries

Sodium-ion batteries are emerging as a complement to lithium-ion technology for stationary storage and low-cost vehicles. The evidence base for their modeling and state estimation is considerably smaller than that for lithium-ion cells and should be maintained separately [28]. Sodium-ion cells with hard-carbon anodes exhibit an open-circuit voltage–state-of-charge (OCV–SOC) curve characterized by a sloping region and a low-slope quasi-plateau, pronounced voltage hysteresis, and impedance and aging mechanisms distinct from those of graphite-based cells [28]. Table 7 summarizes which elements of the lithium-ion methodology are directly transferable and which require the development of new models.

Table 7. Transferability of lithium-ion modeling, identification and estimation methods to sodium-ion.

Element	Directly Transferable	Requires Adaptation	Requires New Models or Data
Identification method (Equations (6)–(8), Figure 5)	Optimizers, constraints, metrics and statistical protocol are model agnostic	Bounds and constraints for sodium-ion parameter ranges	NA
ECM structure	R_0 + RC branches as a structural template	Model order; parameters re-identified over SOC and temperature	Hysteresis states are essential rather than optional
Electrochemical models	The P2D framework in form	Transport and kinetic parameters	Solid-phase storage models for hard carbon; few measured parameters available
Aging	SOH definitions and estimation pipelines	Features (e.g., incremental capacity) must be derived	Degradation models for sodium-specific aging mechanisms; long-term datasets
AI estimators	Architectures and training procedures	Transfer learning from Li-ion data	Public Na-ion datasets for training and benchmarking

7.3. Standardized Open Benchmarks

The fragmented nature of current benchmarking precludes meaningful cross-study comparisons. The community needs a defined set of open benchmarks, similar to those used in the computer vision sector. This suite should mix public datasets with predefined identification and estimation tasks [9], statistical methods and computing budgets. Establishing such a paradigm would reorient academic incentives, shifting the emphasis away from superficial metaphorical novelty and toward measurable, repeatable engineering progress.

7.4. Sample-Efficient and Surrogate-Assisted Identification

Because evaluating complex physical models requires substantial computing power, brute-force population-based metaheuristics are not always the best choice. Future research should systematically compare metaheuristics to sample-efficient alternatives, such as Bayesian optimization and trust-region surrogate methods, on strict, equal computation budgets [76]. In addition, using trained neural simulators in the optimization process can greatly reduce function evaluation times while still keeping physical accuracy.

7.5. Hybrid Neural–Physical Estimators

Purely data-driven approaches often fail to generalize beyond their training distributions, which can introduce substantial safety risks in field deployments. On the other hand, hybrid approaches, including Neural ODE, or estimators regularized with PINNs, are among the most promising directions for robust SOH estimation [16,17,93]. These hybrid systems maintain interpretable physical states while simultaneously learning complex, unmodeled residual dynamics from data, and may therefore help to close the gap between laboratory accuracy and field reliability.

7.6. Uncertainty-Aware and Safety-Certified Estimation

Deterministic point estimates of SOC and SOH are insufficient for safety-critical BMS applications. Advanced AI estimators must incorporate uncertainty quantification [90]. Methods such as conformal prediction, deep ensembles, and Bayesian final layers provide calibrated confidence intervals. These probabilistic outputs are crucial for integrating AI models into systems that must meet stringent functional safety requirements (e.g., ISO 26262).

7.7. Fast-Charging and Second-Life Applications

Battery modeling is moving beyond passive monitoring and toward optimization-in-the-loop applications [43]. Advanced use cases, such as fast charging with lithium plating limitations or rapid electrochemical screening for second-life batteries, require high-accuracy models. Often, parameter identification errors lead to reduced safety margins or loss of economic value, which shows why the thorough validation processes in this study are so important.

8. Conclusions

This review had three main objectives. The summary below explains how each one was met and highlights the key findings.

Objective 1 (integrated appraisal) was addressed in Sections 2–5. Four principal findings are identified. First, the optimal ECM structure depends on both chemistry and profile. The 2RC model is a reasonable default for dynamic automotive profiles, but it does not represent a definitive optimum (Section 2.1). Second, metaheuristics are most effective for multimodal, higher-order, or fractional-order identification problems. For low-order models with informative data, deterministic methods are sufficient, and no single algorithm consistently outperforms others across studies (Section 3.3). Third, for computationally expensive electrochemical models, sample-efficient methods are competitive. For example, in one study, Bayesian Optimization (BO) reduced the mean testing loss by 5.8% and its variance by 72.7% compared to Particle Swarm Optimization (PSO) (Section 3.3). Fourth, artificial intelligence (AI) estimators now routinely achieve state-of-charge (SOC) errors of 1–2% on laboratory drive cycles. However, evidence from field data, calibrated uncertainty, and cross-chemistry transfer remains limited (Section 4). Among the four interfaces between the two methodological families, learned surrogates in identification loops and pipeline optimization demonstrate the most significant benefits (Section 5.1).

Objective 2 (methodological weaknesses) was addressed in Sections 3.5, 4.5 and 6. Five primary pitfalls were identified: algorithm inflation without mechanism-level novelty, in-sample evaluation and data leakage, lack of statistical testing with unequal budgets, neglect of embedded feasibility, and excessive reliance on output error. For each pitfall, supporting evidence and recommended practices were provided (Table 5). Quantitative hardware evidence indicates that small recurrent networks and extended Kalman filters (EKFs) operate within sub-millisecond to tens-of-millisecond computational budgets and

require only a few kilobytes of RAM on microcontrollers. Additionally, quantization can alter accuracy rankings (Table 6).

Objective 3, which concerns practical guidance and the research agenda, was addressed in Sections 5 and 7. This was achieved through a decision map for selecting identification methods (Figure 5), a synthesis matrix that links model and estimator classes to battery management system (BMS) tasks (Table 4), and a research agenda. The agenda addresses standardized benchmarks, sample-efficient identification, hybrid neural–physical estimators, calibrated uncertainty, and chemistry transfer. It also provides a separate evaluation of transferability to sodium-ion cells (Table 7).

This review has several inherent limitations. As a critical narrative review rather than a meta-analysis, heterogeneity in chemistries, profiles, and metrics prevented pooled statistics. The literature search was limited to English-language sources within the databases listed in Table 1. Furthermore, publication bias favoring positive results is likely present in both bodies of literature. Nevertheless, the evidence supports an integrative approach: physically structured models identified through sample-efficient optimization, refined by learning components with quantified uncertainty, and evaluated using open benchmarks that include diverse chemistries, field conditions, and embedded hardware.

Author Contributions: Conceptualization, A.M.N. and H.M.B.; methodology, A.M.N. and M.A.E.; software, A.M.N. and H.M.B.; validation, A.M.N., H.M.B. and M.A.E.; formal analysis, A.M.N. and H.M.B.; investigation, A.M.N. and M.A.E.; resources, A.M.N.; data curation, A.M.N., H.M.B. and M.A.E.; writing—original draft preparation, A.M.N. and H.M.B.; writing—review and editing, A.M.N., H.M.B. and M.A.E.; visualization, A.M.N. and M.A.E.; supervision, A.M.N.; project administration, A.M.N.; funding acquisition, A.M.N. All authors have read and agreed to the published version of the manuscript.

Funding: This research was funded by Prince Sattam bin Abdulaziz University grant number PSAU/2025/RV/11.

Data Availability Statement: No new experimental data were generated in this study.

Acknowledgments: The authors extended their appreciation to Prince Sattam bin Abdulaziz University for funding this research work through the project number PSAU/2025/RV/11.

Conflicts of Interest: The authors declare no conflict of interest.

Abbreviations

The following abbreviations are used in this manuscript:

AEKF	Adaptive extended Kalman filter
AI	Artificial intelligence
ANFIS	Adaptive neuro-fuzzy inference system
AOA	Arithmetic optimization algorithm
APO	Arctic puffin optimization
BMS	Battery management system
BNN	Bayesian neural network
BO	Bayesian optimization
CC	Coulomb counting
CC-CV	Constant current–constant voltage
CMA-ES	Covariance matrix adaptation evolution strategy
CMABO	Classification-model-assisted Bayesian optimization
CNN	Convolutional neural network
CPE	Constant-phase element
CS	Cuckoo search
DE	Differential evolution
DFN	Doyle–Fuller–Newman (model)
DL	Deep learning

DOLADE	Adaptive differential evolution with dynamic opposite learning
DST	Dynamic stress test
ECM	Equivalent circuit model
EIS	Electrochemical impedance spectroscopy
EKF	Extended Kalman filter
ELM	Extreme learning machine
EOLSO	Elite opposition-based learning snake optimization
EV	Electric vehicle
FCNN	Fully connected neural network
FNN	Feedforward neural network
FO	Fractional order
FO-ECM	Fractional-order equivalent circuit model
FP32	32-bit floating point
FUDS	Federal urban driving schedule
GA	Genetic algorithm
GBO	Gradient-based optimizer
GJO	Golden jackal optimization
GL	Grünwald–Letnikov
GPR	Gaussian process regression
GRU	Gated recurrent unit
GWO	Grey wolf optimizer
HBA	Honey badger algorithm
HOA	Hiking optimization algorithm
HPPC	Hybrid pulse power characterization
HS	Harmony search
HWFET	Highway fuel economy test
IC	Incremental capacity
INT8	8-bit integer
JS	Jellyfish search
KF	Kalman filter
LCO	Lithium cobalt oxide ($LiCoO_2$)
LFP	Lithium iron phosphate ($LiFePO_4$)
LIB	Lithium-ion battery
LM	Levenberg–Marquardt
LMO	Lithium manganese oxide
LS	Least squares
LSTM	Long short-term memory
MAE	Mean absolute error
MAPE	Mean absolute percentage error
MaxAE	Maximum absolute error
MC	Monte Carlo
MCU	Microcontroller unit
MLP	Multilayer perceptron
MPA	Marine predators algorithm
MRFO	Manta ray foraging optimization
MSE	Mean squared error
NCA	Lithium nickel cobalt aluminum oxide
NFL	No free lunch
NMC	Lithium nickel manganese cobalt oxide
OBD	On-board diagnostics
OCV	Open-circuit voltage
ODE	Ordinary differential equation
P2D	Pseudo-two-dimensional (model)
PDD	Potential and current-density distribution (model)
PINN	Physics-informed neural network
PLO	Polar lights optimizer
PSO	Particle swarm optimization
RAM	Random-access memory
RBF	Radial basis function
RC	Resistor–capacitor
RLS	Recursive least squares
RMSE	Root mean square error
RMSPE	Root mean square percentage error
RNN	Recurrent neural network

RTH	Red-tailed hawk (algorithm)
RUL	Remaining useful life
SA	Simulated annealing
SaBO	Self-adaptive bonobo optimizer
SCA	Sine–cosine algorithm
SEI	Solid-electrolyte interphase
SO	Snake optimizer
SOC	State of charge
SOH	State of health
SOP	State of power
SPM	Single-particle model
SPMe	Single-particle model with electrolyte dynamics
SSA	Salp swarm algorithm
SSE	Sum of squared errors
TCN	Temporal convolutional network
TLBO	Teaching–learning-based optimization
UDDS	Urban dynamometer driving schedule
UKF	Unscented Kalman filter
WLTC	Worldwide harmonized light vehicle test cycle
WOA	Whale optimization algorithm

Symbols

The following symbols are used in this manuscript:

C_j	Capacitance of the j-th RC branch (F)
d	Dimension of the parameter vector
D^{α}	Fractional derivative of order α
$i(k)$	Cell current, positive for discharge (A)
$J(\theta)$	Identification cost function (V^2)
L	Memory length of the Grünwald–Letnikov approximation (samples)
N	Number of samples
n	Number of RC branches
$OCV(SOC, T)$	Open-circuit voltage as a function of SOC and temperature (V)
$P(\theta)$	Penalty for violation of physical plausibility
Q	CPE coefficient ($F \cdot s^{\alpha-1}$)
Q_n	Nominal capacity (Ah)
R_0	Ohmic resistance (Ω)
R_j	Resistance of the j-th RC branch (Ω)
s	Laplace variable
T	Temperature (°C or K)
$v_j(k)$	Polarization voltage of the j-th RC branch (V)
$v_{meas}(k)$, $v_{model}(k;\theta)$	Measured and simulated terminal voltage (V)
$v_t(k)$	Terminal voltage (V)
$SOC(k)$	State of charge
$Z_{CPE}(s)$	Impedance of a constant-phase element (Ω)
α	CPE dispersion exponent/fractional order (–)
Δt	Sampling period (s)
η	Coulombic efficiency (–)
θ	Identified parameter vector
θ_{min}, θ_{max}	Lower and upper parameter bounds
λ	Penalty weight
τ_j	Time constant of the jth RC branch, $\tau_j = R_j C_j (s)$

Appendix A

Table A1. Summary of the literature search and selection protocol.

Item	Details
Databases	Scopus, WoS Core Collection, IEEE Xplore and ScienceDirect.
Publication time window	Mainly from 2010 to 2026; earlier foundational studies were included to define methods.

Table A1. *Cont.*

Item		Details
Search string	Identification	("lithium-ion" OR "Li-ion") AND ("parameter identification" OR "parameter estimation" OR "model identification") AND (metaheuristic)
	Estimation	("lithium-ion" OR battery) AND ("state of charge" OR "state of health" OR "remaining useful life") AND ("deep learning" OR "neural network" OR "Gaussian process" OR "physics-informed" OR "neural ODE")
	Synergy & deployment	("lithium-ion" OR battery) AND (("hyperparameter" OR surrogate) AND (metaheuristic) OR (microcontroller OR embedded OR "processor-in-the-loop"))
Inclusion criteria		Peer-reviewed journal or conference papers in English; lithium-ion cell or pack applications (sodium-ion only for Section 7.2); identification or estimation results using experimental or public data; review papers for context enhancement.
Exclusion criteria		Non-battery applications (except papers that introduce an algorithm discussed here); materials-scale works; inaccessible full texts.
Classification		Studies were categorized according to the model classes described in Section 2, the algorithm families outlined in Section 3.2 (classified by search mechanism), and the AI architecture classes detailed in Section 4.2. Ambiguous cases were resolved through consensus among the authors.

References

1. Wang, Y.; Tian, J.; Sun, Z.; Wang, L.; Xu, R.; Li, M.; Chen, Z. A Comprehensive Review of Battery Modeling and State Estimation Approaches for Advanced Battery Management Systems. *Renew. Sustain. Energy Rev.* **2020**, *131*, 110015. [CrossRef]
2. Xiong, R.; Cao, J.; Yu, Q.; He, H.; Sun, F. Critical Review on the Battery State of Charge Estimation Methods for Electric Vehicles. *IEEE Access* **2018**, *6*, 1832–1843. [CrossRef]
3. Doyle, M.; Fuller, T.F.; Newman, J. Modeling of Galvanostatic Charge and Discharge of the Lithium/Polymer/Insertion Cell. *J. Electrochem. Soc.* **1993**, *140*, 1526–1533. [CrossRef]
4. Moura, S.J.; Argomedo, F.B.; Klein, R.; Mirtabatabaei, A.; Krstic, M. Battery State Estimation for a Single Particle Model with Electrolyte Dynamics. *IEEE Trans. Contr. Syst. Technol.* **2017**, *25*, 453–468. [CrossRef]
5. He, H.; Xiong, R.; Fan, J. Evaluation of Lithium-Ion Battery Equivalent Circuit Models for State of Charge Estimation by an Experimental Approach. *Energies* **2011**, *4*, 582–598. [CrossRef]
6. Hu, X.; Li, S.; Peng, H. A Comparative Study of Equivalent Circuit Models for Li-Ion Batteries. *J. Power Sources* **2012**, *198*, 359–367. [CrossRef]
7. Wang, B.; Li, S.E.; Peng, H.; Liu, Z. Fractional-Order Modeling and Parameter Identification for Lithium-Ion Batteries. *J. Power Sources* **2015**, *293*, 151–161. [CrossRef]
8. Wang, Y.; Li, M.; Chen, Z. Experimental Study of Fractional-Order Models for Lithium-Ion Battery and Ultra-Capacitor: Modeling, System Identification, and Validation. *Appl. Energy* **2020**, *278*, 115736. [CrossRef]
9. Severson, K.A.; Attia, P.M.; Jin, N.; Perkins, N.; Jiang, B.; Yang, Z.; Chen, M.H.; Aykol, M.; Herring, P.K.; Fraggedakis, D.; et al. Data-Driven Prediction of Battery Cycle Life before Capacity Degradation. *Nat. Energy* **2019**, *4*, 383–391. [CrossRef]
10. Chemali, E.; Kollmeyer, P.J.; Preindl, M.; Ahmed, R.; Emadi, A. Long Short-Term Memory Networks for Accurate State-of-Charge Estimation of Li-Ion Batteries. *IEEE Trans. Ind. Electron.* **2018**, *65*, 6730–6739. [CrossRef]
11. Yang, F.; Song, X.; Xu, F.; Tsui, K.-L. State-of-Charge Estimation of Lithium-Ion Batteries via Long Short-Term Memory Network. *IEEE Access* **2019**, *7*, 53792–53799. [CrossRef]
12. Bairwa, B.; Pareek, K.; Jadoun, V.K. Cycle Based State of Health Estimation of Lithium Ion Cells Using Deep Learning Architectures. *Sci. Rep.* **2025**, *15*, 37078. [CrossRef] [PubMed]
13. Hannan, M.A.; How, D.N.T.; Lipu, M.S.H.; Mansor, M.; Ker, P.J.; Dong, Z.Y.; Sahari, K.S.M.; Tiong, S.K.; Muttaqi, K.M.; Mahlia, T.M.I.; et al. Deep Learning Approach towards Accurate State of Charge Estimation for Lithium-Ion Batteries Using Self-Supervised Transformer Model. *Sci. Rep.* **2021**, *11*, 19541. [CrossRef] [PubMed]
14. Richardson, R.R.; Osborne, M.A.; Howey, D.A. Gaussian Process Regression for Forecasting Battery State of Health. *J. Power Sources* **2017**, *357*, 209–219. [CrossRef]
15. Raissi, M.; Perdikaris, P.; Karniadakis, G.E. Physics-Informed Neural Networks: A Deep Learning Framework for Solving Forward and Inverse Problems Involving Nonlinear Partial Differential Equations. *J. Comput. Phys.* **2019**, *378*, 686–707. [CrossRef]
16. Pepe, S.; Liu, J.; Quattrocchi, E.; Ciucci, F. Neural Ordinary Differential Equations and Recurrent Neural Networks for Predicting the State of Health of Batteries. *J. Energy Storage* **2022**, *50*, 104209. [CrossRef]

17. Aykol, M.; Gopal, C.B.; Anapolsky, A.; Herring, P.K.; Van Vlijmen, B.; Berliner, M.D.; Bazant, M.Z.; Braatz, R.D.; Chueh, W.C.; Storey, B.D. Perspective—Combining Physics and Machine Learning to Predict Battery Lifetime. *J. Electrochem. Soc.* **2021**, *168*, 030525. [CrossRef]
18. Sörensen, K. Metaheuristics—The Metaphor Exposed. *Int. Trans. Oper. Res.* **2015**, *22*, 3–18. [CrossRef]
19. Camacho-Villalón, C.L.; Dorigo, M.; Stützle, T. Exposing the Grey Wolf, Moth-flame, Whale, Firefly, Bat, and Antlion Algorithms: Six Misleading Optimization Techniques Inspired by *Bestial* Metaphors. *Int. Trans. Oper. Res.* **2023**, *30*, 2945–2971. [CrossRef]
20. Mohamed, M.A.A.; Yu, T.F.; Ramsden, G.; Marco, J.; Grandjean, T. Advancements in Parameter Estimation Techniques for 1RC and 2RC Equivalent Circuit Models of Lithium-Ion Batteries: A Comprehensive Review. *J. Energy Storage* **2025**, *113*, 115581. [CrossRef]
21. Peng, J.; Meng, J.; Wu, J.; Deng, Z.; Lin, M.; Mao, S.; Stroe, D.-I. A Comprehensive Overview and Comparison of Parameter Benchmark Methods for Lithium-Ion Battery Application. *J. Energy Storage* **2023**, *71*, 108197. [CrossRef]
22. Wu, Y.; Bai, D.; Zhang, K.; Li, Y.; Yang, F. Advancements in the Estimation of the State of Charge of Lithium-Ion Battery: A Comprehensive Review of Traditional and Deep Learning Approaches. *J. Mater. Inf.* **2025**, *5*, 18. [CrossRef]
23. How, D.N.T.; Hannan, M.A.; Hossain Lipu, M.S.; Ker, P.J. State of Charge Estimation for Lithium-Ion Batteries Using Model-Based and Data-Driven Methods: A Review. *IEEE Access* **2019**, *7*, 136116–136136. [CrossRef]
24. Liu, C.; Li, H.; Li, K.; Wu, Y.; Lv, B. Deep Learning for State of Health Estimation of Lithium-Ion Batteries in Electric Vehicles: A Systematic Review. *Energies* **2025**, *18*, 1463. [CrossRef]
25. Wang, Y.; Guo, S.; Cui, Y.; Deng, L.; Zhao, L.; Li, J.; Wang, Z. A Comprehensive Review of Machine Learning-Based State of Health Estimation for Lithium-Ion Batteries: Data, Features, Algorithms, and Future Challenges. *Renew. Sustain. Energy Rev.* **2025**, *224*, 116125. [CrossRef]
26. Kumar, D.; Nasimov, R.; Singh, A.; Jha, A.; Jha, A.; Rizwan, M. Artificial Intelligence Approaches for SOH Estimation in Lithium-Ion Batteries: A Comprehensive Review of Progress, Critical Evaluations, Challenges, and Toward Future Outlooks. *Appl. Comput. Intell. Soft Comput.* **2025**, *2025*, 5516151. [CrossRef]
27. Chen, H.; Chen, Y.; Sun, C.; Huo, L.; Zhang, W.; Shen, P.; Huang, L.; Luan, W.; Chen, H. Towards Practical Data-Driven Battery State of Health Estimation: Advancements and Insights Targeting Real-World Data. *J. Energy Chem.* **2025**, *110*, 657–680. [CrossRef]
28. Sandri, C.; Di Rienzo, R.; Deiaco, A.; Morelli, M.; Cristofoli, G.; Cazzanti, S.; Baronti, F.; Roncella, R.; Saletti, R. Sodium-Ion Batteries: A Review of Modeling, Safety, and State Estimation Techniques. *J. Energy Storage* **2026**, *163*, 122120. [CrossRef]
29. Page, M.J.; McKenzie, J.E.; Bossuyt, P.M.; Boutron, I.; Hoffmann, T.C.; Mulrow, C.D.; Shamseer, L.; Tetzlaff, J.M.; Akl, E.A.; Brennan, S.E.; et al. The PRISMA 2020 Statement: An Updated Guideline for Reporting Systematic Reviews. *BMJ* **2021**, *372*, n71. [CrossRef] [PubMed]
30. Nejad, S.; Gladwin, D.T.; Stone, D.A. A Systematic Review of Lumped-Parameter Equivalent Circuit Models for Real-Time Estimation of Lithium-Ion Battery States. *J. Power Sources* **2016**, *316*, 183–196. [CrossRef]
31. Tran, M.-K.; DaCosta, A.; Mevawalla, A.; Panchal, S.; Fowler, M. Comparative Study of Equivalent Circuit Models Performance in Four Common Lithium-Ion Batteries: LFP, NMC, LMO, NCA. *Batteries* **2021**, *7*, 51. [CrossRef]
32. Yu, Q.-Q.; Xiong, R.; Wang, L.-Y.; Lin, C. A Comparative Study on Open Circuit Voltage Models for Lithium-Ion Batteries. *Chin. J. Mech. Eng.* **2018**, *31*, 65. [CrossRef]
33. Pillai, P.; Nguyen, J.; Balasingam, B. Performance Analysis of Empirical Open-Circuit Voltage Modeling in Lithium-Ion Batteries—Part 3: Experimental Results. *IEEE Trans. Transp. Electrif.* **2024**, *10*, 7258–7274. [CrossRef]
34. Plett, G.L. *Battery Management Systems*; Artech House Power Engineering Series; Artech House: Boston, MA, USA, 2016.
35. Plett, G.L. Extended Kalman Filtering for Battery Management Systems of LiPB-Based HEV Battery Packs. *J. Power Sources* **2004**, *134*, 277–292. [CrossRef]
36. Podlubny, I. *Fractional Differential Equations: An Introduction to Fractional Derivatives, Fractional Differential Equations, to Methods of Their Solution and Some of Their Applications*; Mathematics in Science and Engineering; Academic Press: San Diego, CA, USA, 1999.
37. Oustaloup, A.; Levron, F.; Mathieu, B.; Nanot, F.M. Frequency-Band Complex Noninteger Differentiator: Characterization and Synthesis. *IEEE Trans. Circuits Syst. I* **2000**, *47*, 25–39. [CrossRef]
38. Yu, M.; Li, Y.; Podlubny, I.; Gong, F.; Sun, Y.; Zhang, Q.; Shang, Y.; Duan, B.; Zhang, C. Fractional-Order Modeling of Lithium-Ion Batteries Using Additive Noise Assisted Modeling and Correlative Information Criterion. *J. Adv. Res.* **2020**, *25*, 49–56. [CrossRef] [PubMed]
39. Tian, J.; Xiong, R.; Shen, W.; Wang, J. A Comparative Study of Fractional Order Models on State of Charge Estimation for Lithium Ion Batteries. *Chin. J. Mech. Eng.* **2020**, *33*, 51. [CrossRef]
40. Wang, S.-C.; Liu, Y.-H. Research on Two-Stage Parameter Identification for Various Lithium-Ion Battery Models Using Bio-Inspired Optimization Algorithms. *Appl. Sci.* **2025**, *16*, 202. [CrossRef]
41. Wang, J.; Yu, W.; Cheng, G.; Chen, L. Identification of Fractional-Order Equivalent Circuit Model of Lithium-Ion Battery for Improving Estimation of State of Charge. *J. Energy Storage* **2023**, *70*, 108043. [CrossRef]

42. Fan, Y.; Zhang, Z.; Yang, G.; Pan, T.; Tian, J.; Li, M.; Liu, X.; Wang, P. A Comparative Study of Modeling and Parameter Identification for Lithium-Ion Batteries in Energy Storage Systems. *Measurement* **2025**, *243*, 116263. [CrossRef]
43. Attia, P.M.; Grover, A.; Jin, N.; Severson, K.A.; Markov, T.M.; Liao, Y.-H.; Chen, M.H.; Cheong, B.; Perkins, N.; Yang, Z.; et al. Closed-Loop Optimization of Fast-Charging Protocols for Batteries with Machine Learning. *Nature* **2020**, *578*, 397–402. [CrossRef] [PubMed]
44. Zhang, Q.; Wang, D.; Yang, B.; Cui, X.; Li, X. Electrochemical Model of Lithium-Ion Battery for Wide Frequency Range Applications. *Electrochim. Acta* **2020**, *343*, 136094. [CrossRef]
45. Bizeray, A.M.; Kim, J.-H.; Duncan, S.R.; Howey, D.A. Identifiability and Parameter Estimation of the Single Particle Lithium-Ion Battery Model. *IEEE Trans. Contr. Syst. Technol.* **2019**, *27*, 1862–1877. [CrossRef]
46. Li, Y.; Liu, G.; Deng, W.; Li, Z. Comparative Study on Parameter Identification of an Electrochemical Model for Lithium-Ion Batteries via Meta-Heuristic Methods. *Appl. Energy* **2024**, *367*, 123437. [CrossRef]
47. Lai, Q.; Ahn, H.J.; Kim, Y.; Kim, Y.N.; Lin, X. New Data Optimization Framework for Parameter Estimation under Uncertainties with Application to Lithium-Ion Battery. *Appl. Energy* **2021**, *295*, 117034. [CrossRef]
48. Ozkan, M.F.; Da Silva, S.F.; El Idrissi, F.; Ramesh, P.; Canova, M. Optimal Design of Experiment for Electrochemical Parameter Identification of Li-Ion Battery via Deep Reinforcement Learning. In *Proceedings of the 2025 IEEE Conference on Control Technology and Applications (CCTA)*; IEEE: San Diego, CA, USA, 2025; pp. 83–88.
49. Saha, B.; Goebel, K. *Battery Data Set*; NASA Ames Prognostics Data Repository, NASA Ames Research Center: Moffett Field, CA, USA, 2007. Available online: http://ti.arc.nasa.gov/project/prognostic-data-repository (accessed on 17 August 2026).
50. He, W.; Williard, N.; Osterman, M.; Pecht, M. Prognostics of Lithium-Ion Batteries Based on Dempster–Shafer Theory and the Bayesian Monte Carlo Method. *J. Power Sources* **2011**, *196*, 10314–10321. [CrossRef]
51. Kollmeyer, P. Panasonic 18650PF Li-ion Battery Data; Mendeley Data, V1, 2018. Available online: https://data.mendeley.com/datasets/wykht8y7tg/1 (accessed on 17 August 2026). [CrossRef]
52. Luh, M.; Blank, T. Comprehensive Battery Aging Dataset: Capacity and Impedance Fade Measurements of a Lithium-Ion NMC/C-SiO Cell. *Sci. Data* **2024**, *11*, 1004. [CrossRef] [PubMed]
53. Birkl, C.R.; Roberts, M.R.; McTurk, E.; Bruce, P.G.; Howey, D.A. Degradation Diagnostics for Lithium Ion Cells. *J. Power Sources* **2017**, *341*, 373–386. [CrossRef]
54. Sangwan, V.; Sharma, A.; Kumar, R.; Rathore, A.K. Estimation of Battery Parameters of the Equivalent Circuit Models Using Meta-Heuristic Techniques. In *Proceedings of the 2016 IEEE 1st International Conference on Power Electronics, Intelligent Control and Energy Systems (ICPEICES)*; IEEE: Delhi, India, 2016; pp. 1–6.
55. Brand, J.; Zhang, Z.; Agarwal, R.K. Extraction of Battery Parameters of the Equivalent Circuit Model Using a Multi-Objective Genetic Algorithm. *J. Power Sources* **2014**, *247*, 729–737. [CrossRef]
56. Tzanetos, A.; Dounias, G. Nature Inspired Optimization Algorithms or Simply Variations of Metaheuristics? *Artif. Intell. Rev.* **2021**, *54*, 1841–1862. [CrossRef]
57. Holland, J.H. *Adaptation in Natural and Artificial Systems: An Introductory Analysis with Applications to Biology, Control, and Artificial Intelligence*; The MIT Press: Cambridge, MA, USA, 1992. [CrossRef]
58. Storn, R.; Price, K. Differential Evolution—A Simple and Efficient Heuristic for Global Optimization over Continuous Spaces. *J. Glob. Optim.* **1997**, *11*, 341–359. [CrossRef]
59. Zhou, J.; Zhang, Y.; Guo, Y.; Feng, W.; Menhas, M.I.; Zhang, Y. Parameters Identification of Battery Model Using a Novel Differential Evolution Algorithm Variant. *Front. Energy Res.* **2022**, *10*, 794732. [CrossRef]
60. Kennedy, J.; Eberhart, R. Particle Swarm Optimization. In *Proceedings of the ICNN'95—International Conference on Neural Networks*; IEEE: Perth, WA, Australia, 1995; Volume 4, pp. 1942–1948.
61. Sepúlveda, J.S.S.; Sepúlveda-Oviedo, E.H.; Jammes, B.; Alonso, C. Parameter Identification of Lithium-Ion Batteries: A Comparative Study of Various Models and Optimization Techniques for Battery Modeling. *arXiv* **2025**. [CrossRef]
62. Mirjalili, S.; Mirjalili, S.M.; Lewis, A. Grey Wolf Optimizer. *Adv. Eng. Softw.* **2014**, *69*, 46–61. [CrossRef]
63. Mirjalili, S.; Lewis, A. The Whale Optimization Algorithm. *Adv. Eng. Softw.* **2016**, *95*, 51–67. [CrossRef]
64. Mirjalili, S.; Gandomi, A.H.; Mirjalili, S.Z.; Saremi, S.; Faris, H.; Mirjalili, S.M. Salp Swarm Algorithm: A Bio-Inspired Optimizer for Engineering Design Problems. *Adv. Eng. Softw.* **2017**, *114*, 163–191. [CrossRef]
65. Chen, B.-J.; Lin, J.-H.; Cheng, Y.-S.; Fang, J.-H.; Liu, Y.-H. Parameter Identification of the Parameters of Lithium-Ion Battery Model Based on Metaheuristic Algorithms. In *Proceedings of the 2024 16th IIAI International Congress on Advanced Applied Informatics (IIAI-AAI)*; IEEE: Takamatsu, Japan, 2024; pp. 724–725.
66. Ghadbane, H.E.; Rezk, H.; Ferahtia, S.; Barkat, S.; Al-Dhaifallah, M. Optimal Parameter Identification Strategy Applied to Lithium-Ion Battery Model for Electric Vehicles Using Drive Cycle Data. *Energy Rep.* **2024**, *11*, 2049–2058. [CrossRef]
67. Turki Almousa, M.; Gomaa, M.R.; Ghasemi, M.; Louzazni, M. Gradient-Based Optimization for Parameter Identification of Lithium-Ion Battery Model for Electric Vehicles. *Results Eng.* **2024**, *24*, 102845. [CrossRef]

68. Li, W.; Xiong, Y.; Zhang, S.; Fan, X.; Wang, R.; Wong, P. A Novel Method of Parameter Identification for Lithium-Ion Batteries Based on Elite Opposition-Based Learning Snake Optimization. *WEVJ* **2025**, *16*, 268. [CrossRef]
69. Ashraf, H.; Abdellatif, S.O.; Elkholy, M.M.; El-Fergany, A.A. Honey Badger Optimizer for Extracting the Ungiven Parameters of PEMFC Model: Steady-State Assessment. *Energy Convers. Manag.* **2022**, *258*, 115521. [CrossRef]
70. Chopra, N.; Mohsin Ansari, M. Golden Jackal Optimization: A Novel Nature-Inspired Optimizer for Engineering Applications. *Expert Syst. Appl.* **2022**, *198*, 116924. [CrossRef]
71. Das, A.K.; Pratihar, D.K. A New Bonobo Optimizer (BO) for Real-Parameter Optimization. In *Proceedings of the 2019 IEEE Region 10 Symposium (TENSYMP)*; IEEE: Kolkata, India, 2019; pp. 108–113.
72. Ferahtia, S.; Houari, A.; Rezk, H.; Djerioui, A.; Machmoum, M.; Motahhir, S.; Ait-Ahmed, M. Red-Tailed Hawk Algorithm for Numerical Optimization and Real-World Problems. *Sci. Rep.* **2023**, *13*, 12950. [CrossRef] [PubMed]
73. Wang, W.; Tian, W.; Xu, D.; Zang, H. Arctic Puffin Optimization: A Bio-Inspired Metaheuristic Algorithm for Solving Engineering Design Optimization. *Adv. Eng. Softw.* **2024**, *195*, 103694. [CrossRef]
74. Oladejo, S.O.; Ekwe, S.O.; Mirjalili, S. The Hiking Optimization Algorithm: A Novel Human-Based Metaheuristic Approach. *Knowl.-Based Syst.* **2024**, *296*, 111880. [CrossRef]
75. Aljaidi, M.; Jangir, P.; Agrawal, S.P.; Pandya, S.B.; Parmar, A.; Gulothungan, G.; Alkoradees, A.F.; Khishe, M.; Jangid, R. Polar Lights Optimizer: A Novel Algorithm for Accurate Parameter Estimation in Proton Exchange Membrane Fuel Cells. *Results Eng.* **2025**, *27*, 106571. [CrossRef]
76. Pi, J.; Da Silva, S.F.; Ozkan, M.F.; Gupta, A.; Canova, M. Parameter Identification for Electrochemical Models of Lithium-Ion Batteries Using Bayesian Optimization. *IFAC-PapersOnLine* **2024**, *58*, 180–185. [CrossRef]
77. Wang, B.-C.; He, Y.-B.; Liu, J.; Luo, B. Fast Parameter Identification of Lithium-Ion Batteries via Classification Model-Assisted Bayesian Optimization. *Energy* **2024**, *288*, 129667. [CrossRef]
78. Shen, W.-J.; Li, H.-X. Multi-Scale Parameter Identification of Lithium-Ion Battery Electric Models Using a PSO-LM Algorithm. *Energies* **2017**, *10*, 432. [CrossRef]
79. Lai, X.; Gao, W.; Zheng, Y.; Ouyang, M.; Li, J.; Han, X.; Zhou, L. A Comparative Study of Global Optimization Methods for Parameter Identification of Different Equivalent Circuit Models for Li-Ion Batteries. *Electrochim. Acta* **2019**, *295*, 1057–1066. [CrossRef]
80. Kalogiannis, T.; Hosen, M.; Sokkeh, M.; Goutam, S.; Jaguemont, J.; Jin, L.; Qiao, G.; Berecibar, M.; Van Mierlo, J. Comparative Study on Parameter Identification Methods for Dual-Polarization Lithium-Ion Equivalent Circuit Model. *Energies* **2019**, *12*, 4031. [CrossRef]
81. Kim, M.; Chun, H.; Kim, J.; Kim, K.; Yu, J.; Kim, T.; Han, S. Data-Efficient Parameter Identification of Electrochemical Lithium-Ion Battery Model Using Deep Bayesian Harmony Search. *Appl. Energy* **2019**, *254*, 113644. [CrossRef]
82. Wolpert, D.H.; Macready, W.G. No Free Lunch Theorems for Optimization. *IEEE Trans. Evol. Comput.* **1997**, *1*, 67–82. [CrossRef]
83. Zhang, C.; Li, K.; Deng, J.; Song, S. Improved Realtime State-of-Charge Estimation of $LiFePO_4$ Battery Based on a Novel Thermoelectric Model. *IEEE Trans. Ind. Electron.* **2017**, *64*, 654–663. [CrossRef]
84. Zhang, S.; Zhang, X. A Comparative Study of Different Online Model Parameters Identification Methods for Lithium-Ion Battery. *Sci. China Technol. Sci.* **2021**, *64*, 2312–2327. [CrossRef]
85. Aranha, C.; Camacho Villalón, C.L.; Campelo, F.; Dorigo, M.; Ruiz, R.; Sevaux, M.; Sörensen, K.; Stützle, T. Metaphor-Based Metaheuristics, a Call for Action: The Elephant in the Room. *Swarm Intell.* **2022**, *16*, 1–6. [CrossRef]
86. Wang, D.; Yang, Y.; Gu, T. A Hierarchical Adaptive Extended Kalman Filter Algorithm for Lithium-Ion Battery State of Charge Estimation. *J. Energy Storage* **2023**, *62*, 106831. [CrossRef]
87. Liu, S.; Deng, D.; Wang, S.; Luo, W.; Takyi-Aninakwa, P.; Qiao, J.; Li, S.; Jin, S.; Hu, C. Dynamic Adaptive Square-Root Unscented Kalman Filter and Rectangular Window Recursive Least Square Method for the Accurate State of Charge Estimation of Lithium-Ion Batteries. *J. Energy Storage* **2023**, *67*, 107603. [CrossRef]
88. Guo, S.; Ma, L. A Comparative Study of Different Deep Learning Algorithms for Lithium-Ion Batteries on State-of-Charge Estimation. *Energy* **2023**, *263*, 125872. [CrossRef]
89. Naguib, M.; Kollmeyer, P.J.; Emadi, A. State of Charge Estimation of Lithium-Ion Batteries: Comparison of GRU, LSTM, and Temporal Convolutional Deep Neural Networks. In *Proceedings of the 2023 IEEE Transportation Electrification Conference & Expo (ITEC)*; IEEE: Detroit, MI, USA, 2023; pp. 1–6.
90. Ke, Y.; Long, M.; Yang, F.; Peng, W. A Bayesian Deep Learning Pipeline for Lithium-ion Battery SOH Estimation with Uncertainty Quantification. *Qual. Reliab. Eng.* **2024**, *40*, 406–427. [CrossRef]
91. Yang, Y.; Xu, Y.; Nie, Y.; Li, J.; Liu, S.; Zhao, L.; Yu, Q.; Zhang, C. Deep Transfer Learning Enables Battery State of Charge and State of Health Estimation. *Energy* **2024**, *294*, 130779. [CrossRef]
92. Wang, T.; Chao, R.; Dong, Z.; Feng, L. Weakly Supervised Battery SOH Estimation With Imprecise Intervals. *IEEE Trans. Energy Convers.* **2025**, *40*, 1841–1855. [CrossRef]

93. Wang, L.; Yang, T.; Hu, B. A Battery State-of-Health Estimation Method for Real-World Electric Vehicles Based on Physics-Informed Neural Networks. *IEEE Sens. J.* **2025**, *25*, 15577–15587. [CrossRef]
94. Ren, X.; Liu, S.; Yu, X.; Dong, X. A Method for State-of-Charge Estimation of Lithium-Ion Batteries Based on PSO-LSTM. *Energy* **2021**, *234*, 121236. [CrossRef]
95. Kim, J.; Chun, H.; Baek, J.; Han, S. Parameter Identification of Lithium-Ion Battery Pseudo-2-Dimensional Models Using Genetic Algorithm and Neural Network Cooperative Optimization. *J. Energy Storage* **2022**, *45*, 103571. [CrossRef]
96. Kuchly, J.; Heitzmann, T.; Mesbahi, T. Embedded Computational Cost Analysis of a Hybrid AI/Physics-Based State-of-Charge Estimation Method for Lithium-Ion Batteries. *IEEE Open J. Veh. Technol.* **2026**, *7*, 1804–1813. [CrossRef]
97. Naguib, M.; Kollmeyer, P.; Vidal, C.; Duque, J.; Gross, O.; Emadi, A. Microprocessor execution time and memory use for battery state of charge estimation algorithms. In *Proceedings of the WCX SAE World Congress Experience, Detroit, MI, USA and Online, 5 April 2022*; Paper No. 2022-01-0697; SAE International: Warrendale, PA, USA, 2022. [CrossRef]
98. Liang, Y.; Lin, X.; Tang, X.; Shen, W.; Wang, J.; Zheng, L. Comparative Study of Embedded Deep Learning Models for State of Charge Estimation of Lithium-Ion Batteries. *World Electr. Veh. J.* **2026**, *17*, 401. [CrossRef]
99. Ali, S.; Bianchi, V.; De Munari, I. A Microcontroller Based Optimized Framework for the State of Charge Estimation of a Lithium Ion Battery. In *Proceedings of the 2025 IEEE International Workshop on Metrology for Automotive (MetroAutomotive)*; IEEE: Parma, Italy, 2025; pp. 257–261.

Disclaimer/Publisher's Note: The statements, opinions and data contained in all publications are solely those of the individual author(s) and contributor(s) and not of MDPI and/or the editor(s). MDPI and/or the editor(s) disclaim responsibility for any injury to people or property resulting from any ideas, methods, instructions or products referred to in the content.